UNIVERSITY OF LJUBLJANA
BIOTECHNICAL FACULTY

Priyanka SINGH

SUPER-RESOLUTION OPTICAL MICROSCOPIC STUDY OF SINGLE VESICLES IN ASTROCYTES

Doctoral Dissertation

Ljubljana, 2014

UNIVERSITY OF LJUBLJANA
BIOTECHNICAL FACULTY

Priyanka SINGH

ŠTUDIJA POSAMEZNIH MEŠIČKOV V ASTROCITIH Z METODO OPTIČNE MIKROSKOPIJE VISOKE LOČLJIVOSTI

DOKTORSKA DISERTACIJA

SUPER-RESOLUTION OPTICAL MICROSCOPIC STUDY OF SINGLE VESICLES IN ASTROCYTES

DOCTORAL DISSERTATION

Ljubljana, 2014

Doctoral dissertation – Cell Sciences under Biosciences doctoral studies at the Biotechnical Faculty, University of Ljubljana. The research work was performed Laboratory Neuroendocrinology – Molecular Cell Physiology, Institute of Pathophysiology, Medical Faculty, University of Ljubljana.

Supervisor: Acad. Prof. Dr. Robert ZOREC
Co-supervisor: Zn. Sod. Dr. Maja POTOKAR

The date of approval for doctoral dissertation is 2nd June, 2014.

The Commission for assessment and defence: 31st March, 2014.

President: Prof. Dr. Marko KREFT
University of Ljubljana, Biotechnical Faculty, Department of Biology

Member: Acad. Prof. Dr. Robert ZOREC
University of Ljubljana, Medical Faculty, Institute of Pathophysiology

Member: Prof. DDr. Aleš IGLIČ
University of Ljubljana, Electrical Engineering Faculty

Member: Zn. Sod. Dr. Maja POTOKAR
University of Ljubljana, Medical Faculty, Institute of Pathophysiology

Date of defence: 17th June, 2014.

Declaration:

The work is the result of my own research work. I agree with publishing of my work in full text on the internet page Digitalna knjižnica Biotehniške fakultete. I declare that the text in the electronic version is identical to the printed one.

Priyanka Singh

KEY WORDS DOCUMENTATION (KWD)

ND Dd
DC UDC 576.3:543.384:537.533.35(043.3)=111
CX astrocytes/SNARE proteins/synaptobrevin/synaptopHluorin/vesicles/ confocal microscopy/structured illumination microscopy
AU SINGH, Priyanka M.Sc. Chem.
AA ZOREC, Robert (supervisor)/POTOKAR, Maja (co-advisor)
PP SI-1000 Ljubljana, Jamnikarjeva 101
PB University of Ljubljana, Biotechnical Faculty, Interdisciplinary Doctoral Study Programme in Biosciences, Scientific Field Cell Sciences
PY 2014
TI SUPER-RESOLUTION OPTICAL MICROSCOPIC STUDY OF SINGLE VESICLES IN ASTROCYTES
DT Doctoral Dissertation
NO XIII, 64 p., 6 tab., 21 fig., 2 ann., 107 ref.
LA En
AL en/sl
AB Exocytic transmitter release is regulated by the SNARE complex, which contains a vesicular protein, synaptobrevin2 (Sb2). However, Sb2 vesicular arrangement is unclear. Using super-resolution optical microscopy, we studied the prevalence and distribution of endogenous and exogenous Sb2 in single vesicles of astrocytes, the most abundant glial cells in the brain. We tagged Sb2 protein at C- and N-termini with a pair of fluorophores, which allowed us to determine the Sb2 length and geometry. To estimate total number of Sb2 proteins per vesicle and the quantity necessary for the formation of fusion pores, we treated cells with ATP to stimulate Ca^{2+}-dependent exocytosis, we increased intracellular alkalinity to enhance the fluorescence presentation of yellow-shifted pHluorin (YpH), appended to the vesicle lumen domain of Sb2 and performed photo bleaching of YpH fluorophores. Fluorescence intensity of the fluorophores, a parameter proportional to the number of fluorescent molecules, revealed the total number of exogenus Sb2 molecules per vesicle as ≤ 5 and the total number of endogenous Sb2 molecules per vesicle is ≤ 25. However, only one of Sb2 molecule appeared necessary for vesicle fusion pore formation during ATP stimulation.

KLJUČNA DOKUMENTACIJSKA INFORMACIJA (KDI)

ŠD	Dd
DK	UDC 576.3:543.384:537.533.35(043.3)=111
KG	Astrociti/proteini SNARE/sinaptobrevini/sinaptopHluorini/mešički/ konfokalna mikroskopija/SIM mikroskopija
AV	SINGH, Priyanka mag. kem.
SA	ZOREC, Robert (mentor)/POTOKAR, Maja (somentor)
KZ	SI-1000 Ljubljana, Jamnikarjeva 101
ZA	Univerza v Ljubljani, Biotehniška fakulteta, Interdisciplinarni doktorski študij Bioznanosti, znanstveno področje Znanosti o celici
LI	2014
IN	ŠTUDIJA POSAMEZNIH MEŠIČKOV V ASTROCITIH Z METODO OPTIČNE MIKROSKOPIJE VISOKE LOČLJIVOSTI
TD	Doktorska Disertacija
OP	XIII, 64 str., 6 pregl., 21 sl., 2 pril., 107 vir.
IJ	En
JI	en/sl
AI	Sproščanje signalnih molekul z eksocitozo uravnava skupina beljakovin, ki tvori t.i. kompleks SNARE. Ena od beljakovin kompleksa SNARE je beljakovina sinapobrevin2 (Sb2), ki se nahaja na mešičkih. Razporeditev in število molekul Sb2 na mešičkih ni poznano. Z visokoločljivostno mikroskopijo smo raziskovali pojavnost in porazdelitev endogene in eksogene beljakovine Sb2 na posameznih mešičkih v astrocitih, najštevilčnejših celicah glije v možganih. Dolžino in geometrijo beljakovine Sb2 smo določili na rekombinantni beljakovini Sb2, ki ima s parom fluoroforjev označen C in N konec molekule. Za oceno števila molekul Sb2 na posameznem mešičku in števila molekul Sb2, ki zadostujejo za nastanek fuzijske pore, smo celicam dodali ATP in tako stimulirali od Ca^{2+} ionov odvisno eksocitozo, zvišali alkalnost celic in tako zvišali intenziteto fluorescence rumene fluorescenčne beljakovine pHluorin (YpH), ki je pripeta na domeno Sb2 v lumnu mešička ter izvedli foto bledenje YpH fluoroforjev. Na osnovi meritev intenzitete fluorescence fluoroforjev, parametra, ki je sorazmeren številu fluorescenčnih molekul, smo ocenili, da je na posameznem mešičku pet ali manj eksogenih molekul Sb2 in petindvajset ali manj endogenih eksogenih molekul Sb2. Po stimulaciji z ATP je zelo verjetno le ena molekula Sb2 dovolj za nastanek fuzijske pore.

TABLE OF CONTENTS

KEY WORDS DOCUMENTATION (KWD).....III

KLJUČNA DOKUMENTACIJSKA INFORMACIJA (KDI).....IV

TABLE OF CONTENTS.....V

INDEX OF TABLES.....VIII

INDEX OF FIGURES.....IX

ABBREVIATIONS AND SYMBOLS.....XI

PUBLICATIONS.....XIII

1 INTRODUCTION.....1

1.1 SCIENTIFIC ISSUE.....1

1.2 OBJECTIVES.....2

1.3 RESEARCH HYPOTHESIS.....2

1.3.1 Synaptobrevin2 (Sb2) molecules are clustered in astrocytic vesicles.....2

1.3.2 Less than ten molecules of Sb2 proteins are present per astrocytic vesicle.....3

1.3.3 Alkalinization after vesicular fusion elicits an increase of fluorescence in a limited portion of all luminal YSpH.....3

2 LITERATURE REVIEW.....4

2.1 ASTROCYTES.....4

2.1.1 Gliotransmitter release by astrocytes.....4

2.1.2 Secretory vesicles.....6

2.2 SYNAPTOBREVIN.....8

2.2.1 SynaptopHluorin.....10

2.3 CONFOCAL LASER SCANNING MICROSCOPY.....12

2.3.1 Diffraction limit.....13

2.4. SUPER-RESOLUTION MICROSCOPY.....15

2.4.1 Structured illumination microscopy.....15

3 MATERIALS AND METHODS.....17

3.1 CELL CULTURE.....17

3.2 PLASMID DNA.....17

3.3 ISOLATION OF PLASMID DNA.....17

3.4 TRANSFECTION OF ASTROCYTES.....18

3.5 IMMUNOCYTOCHEMISTRY.....18

3.5.1 Labelling of different vesicle types.....18

3.5.2 Labelling of Sb2 vesicles for measuring the distance between fluorophores.....18

3.6 OPTICAL IMAGING.....19

3.6.1 Confocal laser scanning microscopy.....19

3.6.2 Structured illumination microscopy.....19

3.7 SINGLE VESICLE PHLUORIN EXPERIMENTS.....19

3.8 PHOTO BLEACHING EXPERIMENTS.....19

3.9 DATA ANALYSIS.....20

3.9.1 Colocalization of fluorophores.....20

3.9.2 Distance and diameter measurements.....20

3.9.3 Data fitting.....20

3.9.4 Statistical significance.....21

4 RESULTS.....22

4.1 VESICLE DIAMETER OF DIFFERENT VESICLE TYPES IN ASTROCYTES.....22

4.2 ARRANGEMENT OF SB2 ON A SINGLE VESICLE IN ASTROCYTES.....24

4.3 DIAMETER MEASUREMENTS OF PHLUORIN-LADEN VESICLES IN ASTROCYTES.....30

4.4 ANALYSIS OF FLUORESCENCE INTENSITY OF ATTO AND YPH FLUOROPHORES.....32

4.5 YSPH EXPRESSION AND THE NUMBER OF SB2 MOLECULES ON SINGLE VESICLES....34

4.6 PHOTO BLEACHING OF YSPH FLUOROSCENCE IN ASTROCYTES.37

4.7 DETERMINATION OF ENDOGENOUS SB2 MOLECULES....40

5 DISCUSSION....42

5.1 NONUNIFORM DISTRIBUTION OF SB2 ON THE VESICLE MEMBRANE....42

5.2 VESICLE DIAMETER BY A LUMEN-FILLING APPROACH....43

5.3 HOW MANY SB2 MOLECULES ARE PRESENT IN AN ASTROCYTIC VESICLE?....43

6 CONCLUSION....46

7 SUMMARY (POVZETEK)....48

7.1 SUMMARY....48

7.2 POVZETEK....52

8 REFERENCES....56

ACKNOWLEGMENTS

TABLE OF ANNEXES

INDEX OF TABLES

Tab. 1: Diameter of different vesicle types, values obtained from EM.....6

Tab. 2: Compilation of vesicle sizes from different cell types.....7

Tab. 3: Diameter of different vesicle types, values estimated from CLSM and SIM...23

Tab. 4: The average (mean ± s.e.m.) of absolute intensities obtained by fittingGaussian curves on green (YpH) and red (Atto) fluorescent puncta.....29

Tab. 5: Stimulation experiment: Area under the curve (*A*) and mean value of each peak (μ) obtained from Gaussian curves by using Levenberg-Marquardt minimization fit.....36

Tab. 6: Photo bleaching experiment: Area under the curve (*A*) and mean value of each peak (μ) obtained from Gaussian curves by using Levenberg-Marquardt minimization fit.....39

INDEX OF FIGURES

Fig. 1: Pictorial view of the SNARE complex.....9

Fig. 2: Structure of synaptobrevin2 (Sb2).....10

Fig. 3: Exocytosis relieves the proton-dependent quenching of ecliptic-pHluorin fluorescence.....11

Fig. 4: Emission spectra of synaptopHluorins.....11

Fig. 5: Schematic of the optical path in confocal laser scanning microscope.....12

Fig. 6: Diffraction limit in confocal microscope.....14

Fig. 7: Concept of resolution enhancement by structured illumination.....15

Fig. 8: Structure of Atto 594 dye.....16

Fig. 9: CLSM images of astrocytes with marked different vesicle types.....22

Fig. 10: SIM images of astrocytes with marked different vesicle types.....23

Fig. 11: Schematic representation of a vesicle-associated membrane protein Sb2 fluorescently labelled at the luminal and cytoplasmic sides of the vesicle membrane.....25

Fig. 12: Comparison of images of cultured rat astrocytes with fluorescently labelled Sb2 at the vesicle lumen and cytoplasmic sites obtained by CLSM and SIM.....26

Fig. 13: Patterns of two Sb2-associated fluorophores, YpH and Atto, reveal nonuniform vesicular distribution of Sb2.....27

Fig. 14: SIM images reveal the distance between two fluorophores.....30

Fig. 15: Measurement of vesicle diameter in live astrocytes recorded by SIM.....31

Fig. 16: Fluorophore intensity distributions indicate multiples of Sb2 molecules per vesicle.....32

Fig. 17: Correlation between fluorescence intensity and area of the Atto punctum.....33

Fig. 18: Stimulation of YSpH-labelled vesicles by ATP and NH_4Cl reveals the number of Sb2 molecules present on a single astrocytic vesicle.....34

Fig. 19: Diameters of astrocytic vesicles expressing YSpH after ATP and NH_4Cl stimulations.....37

Fig. 20: Photo bleaching of YSpH-labelled vesicles confirms the number of Sb2 molecules on a single astrocytic vesicle.....38

Fig. 21: Quantification of the ratio between the number of YSpH and endogenous Sb2 molecules in astrocytic vesicles.....40

ABBREVIATIONS AND SYMBOLS

aa	Amino acid residues
AGM	Astrocyte growth medium
ANP	Atrial natriuretic protein
AT2	Angiotensin 2
ATP	Adenosine triphosphate
BDNF	Brain-derived neurotrophic factor
BSA	Bovine serum albumin
CLSM	Confocal laser scanning microscopy
DMEM	Dulbecco's modified eagle medium
DPC	Dodecylphosphocholine micelles
ECS	Extracellular solution
EEA1	Early endosome antigen 1
EM	Electron microscopy
EMCCD	Electron multiplying charge coupled device
FBS	Fetal bovine serum
FM	N-(3-triethylammoniumpropyl)-4-(4-(dibutylamino) Styryl) pyridium dibromide
FWHM	Full width at half maximum
GFP	Green fluorescent protein
GSpH	Green synaptopHluorin
HEPES	N-2-hydroxyethylpiperazine-N′-2-ethanesulfonic acid
LAMP 1	Lysosomal associated membrane protein 1
LM	Light microscopy
NA	Numerical aperture of a microscope
NH_4Cl	Ammonium chloride
NMDA	N-methyl-D-aspartate receptor
NPY	Neuropeptide Y
NTR	Neurotrophin receptor

PALM	Photoactivated localization microscopy
PBS	Phosphate bovine serum
PSF	Point spread function, three-dimensional intensity distribution of the image of a point object
RCF	Relative centrifugal force
RPM	Revolutions per minute
S. No.	Serial number
Sb2	Synaptobrevin2
SERT	Serotonin transporter
SIM	Structured illumination microscopy
SNARE	N-ethylmaleimide sensitive factor attachment protein receptor
STED	Stimulated emission depletion microscopy
TEP	Two-photon extracellular polar tracer imaging
TH	Tyrosine hydroxylase
TIRF	Total internal reflection microscopy
VAMP 2	Vesicular associated membrane protein 2
VGLUT 1	Vesicular glutamate transporter 1
YFP	Yellow fluorescent protein
YpH	Yellow pHluorin protein (pH-sensitive yellow fluorescent protein)
YSpH	Yellow synaptopHluorin (Sb2 with YpH fused to the luminal end)
λ_{em}	Emission wavelength
λ_{ex}	Excitation wavelength
$[Ca^{2+}]$	Concentration of calcium ions

PUBLICATIONS

Singh P., Jorgačevski J., Kreft M., Grubišić V., Stout R. F., Potokar M., Parpura V., Zorec R. 2014. Single-vesicle architecture of synaptobrevin2 in astrocytes. Nature Communications, 5: 3780.

1 INTRODUCTION

1.1 SCIENTIFIC ISSUE

Astrocytes are glial cells that can release a variety of chemical messengers, which are called gliotransmitters. Several gliotransmitters are stored in secretory vesicles and are released into the extracellular space via Ca^{2+}-dependent exocytosis (Parpura et al., 1994). Last steps of the exocytosis involve the formation of an aqueous channel (i.e. the fusion pore), which can reversibly close (transient exocytosis; (Ceccarelli et al., 1973)) or fully open (full fusion exocytosis; (Heuser and Reese, 1973)). Exocytosis is a remarkably fast process in neurons, while in other cell types, including astrocytes it is considerably slower (Kreft et al., 2004). Ca^{2+}-dependent exocytosis is governed by exocytotic secretory proteins such as proteins that form the soluble N-ethyl maleimide-sensitive fusion protein attachment protein receptor (SNARE) complex: synaptobrevin 2 (Sb2), cellubrevin, syntaxins 1, 2 and 4 and synaptosome-associated protein of 23 kDa (SNAP-23), which are expressed also in astrocytes (Gucek et al., 2012). Secretory vesicles containing Sb2 were shown to be present in vicinity of electron-lucent vesicles with diameters ranging from 30 to over 100 nm (Bezzi et al., 2004; Crippa et al., 2006; Maienschein et al., 1999). However, vesicles with diameters over 1 μm have been observed to form after stimulation with glutamate (Xu et al., 2007).

To elucidate the mechanism of exocytosis it is important to learn about the single vesicle architecture in astrocytes. Specifically, there is limited and controversial data available about the number of Sb2 present on a single vesicle membrane (Domanska et al., 2009; Karatekin et al., 2010; Mohrmann et al., 2010; Sinha et al., 2011; Takamori et al., 2006; van den Bogaart et al., 2010) and about the number of Sb2 molecules that are actually involved in the fusion of the vesicle membrane with the plasma membrane (Mohrmann et al., 2010; Sinha et al., 2011; van den Bogaart et al., 2010). Moreover, the size of Sb2 molecule in live astrocytes is not known, nor the arrangement of Sb2 molecules on the vesicle membrane. Finally, all these data has to be correlated with the size of the vesicles containing Sb2, which has been shown to be an important parameter in the vesicular fusion (Jorgacevski et al., 2011).

We studied these issues by using fluorescent proteins and advanced super-resolution fluorescence microscopy.

1.2 OBJECTIVES

- To determine the size of Sb2 protein in live astrocyte.
- To visualize the arrangement of Sb2 molecules on astrocytic vesicles.
- To measure the diameters of vesicles containing Sb2 in astrocytes.
- To estimate the number of Sb2 molecules on a single vesicle in astrocytes.
- To determine the number of Sb2 molecules necessary for vesicular fusion in astrocytes.

1.3 RESEARCH HYPOTHESES

1.3.1 Sb2 molecules are clustered in an astrocytic vesicle

According to the literature, there are seventy Sb2 on a synaptic vesicle (Takamori et al. 2006). α-helices of different Sb2 molecules can form hydrogen bonds, suggesting that, together with electrostatic interactions, they can promote clustering of these molecules (Lehninger, 1975). Further support for clustering has been shown in *in vitro* experiments, by showing that Sb2 tend to dimerize due to the presence of cysteine residue present in α-helix backbone of Sb2 (Laage and Langosch, 1997). However, no data of clustering in vesicles of live cells has been reported yet. The combination of relatively large size of Sb2 molecules (Ellena et al., 2009) and relatively small diameters of synaptic like vesicles of astrocytes (Guček et al., 2012) likely favours afore mentioned clustering of Sb2 molecules. Clustering of Sb2 would significantly affect vesicle docking to the target membranes (e.g. the plasma membrane). Therefore, we propose that clustering of Sb2 molecules occurs in vesicles of live astrocytes.

1.3.2 Less than ten molecules of Sb2 proteins are present per astrocytic vesicle

Even though a study by Takamori and coworkers reports seventy Sb2 per a synaptic vesicle, other studies show that only three (Mohrmann et al., 2010), two (Sinha et al., 2011) or even one (van den Bogaart et al., 2010) Sb2 is sufficient for fusion of vesicle with the plasma membranes in synapses. There is no data about the number of Sb2 present in astrocyte vesicles, nor is there any report suggesting how many Sb2 molecules participate in vesicle fusion in this cell type. The kinetics of vesicle merger with the plasma membrane in astrocytes is significantly slower, compared to the kinetics of this process in neurons (Kreft et al., 2004). If kinetics is related also to the sheer number of available Sb2 molecules, one would expect less Sb2 molecules in astrocytic vesicles, compared to vesicles in neurons. Based on relatively slow kinetics of exocytosis and on low number of

Sb2 molecules needed for this process, we suggest that there are on average less than ten Sb2 molecules present per astrocytic vesicle.

1.3.3 Alkalinization after vesicular fusion elicits an increase of fluorescence in a limited portion of all luminal YSpH

In regulated exocytosis, vesicle fusion with the plasma membrane leads to the release of the vesicle content. It was first proposed that in the process of fusion, the vesicle membrane completely merges with the plasma membrane (i.e. full-fusion exocytosis) (Heuser and Reese, 1973). However, there is an alternative model, where vesicle and plasma membranes fuse transiently (Ceccarelli et al. 1973). Here, a narrow channel termed a fusion pore transiently opens and thus connects the vesicle interior to the cell exterior. During this brief period, which lasts a few tens of milliseconds, protons can effectively diffuse from vesicle lumen (Vardjan et al. 2007). In this mode of exocytosis consequent alkalinization of the vesicle lumen is initialy not uniform, which would potentially promote an increase of fluorescence in a limited portion of luminal pH sensitive fluorescence proteins (e.g. Yellow synaptopHluorin (YSpH)). Transient mode of exocytosis has been observed in astrocytes previously (Bowser and Khakh, 2007; Malarkey et al., 2011). Hence, we propose that alkalinization after vesicular fusion elicits an increase of fluorescence in a limited portion of all luminal YSpH in live astrocytes.

2 LITERATURE REVIEW

2.1 ASTROCYTES

Astrocytes are glial cells which provide important metabolic support to neurons, actively tune synaptic activity and influence brain microcirculation (Nedergaard et al., 2003). They are the third active element in the tripartite structure of a synapse. Astrocytes release a variety of transmitters into the extracellular space using several different mechanisms (Malarkey and Parpura, 2008): (a) Ca^{2+} and SNARE dependent vesicular exocytosis (Parpura et al., 1994), (b) reversal action of glutamate transporters (Szatkowski et al., 1990), (c) transportation by cysteine-glutamate antiporter (Warr et al., 1999), (d) permeation through channels or receptors (Duan et al., 2003), (e) volume regulated anion channel (Kimelberg et al., 1990) and (g) gap junction hemichannel (Ye et al., 2003).

One of the key processes which sustain astrocyte communication with neighbouring cells is regulated exocytosis, which involves the fusion of the vesicle and the plasma membranes. Astrocytes propagate Ca^{2+} waves over long distances in response to stimulation such as ATP and then astrocytes release gliotransmitters in Ca^{2+} dependent manner (Parpura et al., 1994). Our understanding of how astrocytes propagate Ca^{2+} waves has undergone substantial revision during the past few years. Originally, it was believed that Ca^{2+} or inositol triphosphate diffused through gap junction and in a regenerative fashion involving phospholipase C, increased Ca^{2+} levels in neighbouring cells. The role of gap junctions in Ca^{2+}-wave propagation was questioned because of the observation that astrocytes lacking physical contact with other astrocytes also engaged in Ca^{2+} waves; indeed, Ca^{2+} waves appeared to leap over areas of non-contiguity. This suggested that an extracellular component might mediate intercellular Ca^{2+} signalling. ATP was subsequently identified as the diffusible messenger of Ca^{2+} signalling in astrocytes. Astrocytes express the purine receptors P_2Y_1, P_2Y_2, P_2Y_4, P_2X_7 and one or more of these appear to participate in the mobilization of intracellular Ca^{2+} stores during wave propagation.

2.1.1 Gliotransmitter release by astrocytes

One of the principal functions of astrocytes is uptake of neurotransmitters released from nerve terminals. Astrocytes also release amino acids, nucleotides, neuroactive agents including transmitters, eicosanoids, steroids, neuropeptides and growth factors (Melcangi et al., 1997). The regulation and the mechanism of astrocyte-mediated release of neuroactive compounds are the subject of intense research, yet they are still poorly defined. Release of glutamate appears to be the primary mechanism by which astrocytes modulate

synaptic transmission. Astrocytic glutamate release in response to synaptic activity appears dependent on mobilization of intracellular Ca^{2+} stores and is attenuated when intracellular [Ca^{2+}] is stabilized by preloading with either the Ca^{2+} chelator or the Ca^{2+}-ATPase inhibitor.

The evidence for Ca^{2+} -dependent gliotransmitter release from astrocytes was demonstrated for glutamate, which release from astrocytes (Parpura et al., 1994). There are multiple sources of Ca^{2+} for Ca^{2+} -dependent gliotransmitter release from astrocytes. Similarly, Ca^{2+} ionophore-stimulated astrocytes can also release D-serine, a co-agonist of the glycine-binding site of the NMDA receptor (Mothet et al., 2005). In support of ATP being released from astrocytes by Ca^{2+}-dependent exocytosis, astrocytes exposed to nitric oxide showed an increase in cytosolic Ca^{2+} with consequential release of ATP into the ECS (Bal-Price et al., 2002). The release of peptides, e.g. ANP, from cultured astrocytes was demonstrated by monitoring optically fluorescently labelled vesicles in cells exposed to Ca^{2+} ionophore (Krzan et al., 2003).

Despite intense effort, the pathway of glutamate release in this context is not understood. One line of work has suggested that glutamate is released by regulated exocytosis, whereas others have provided evidence for channel-mediated release of glutamate (Han et al., 2013; Woo et al., 2012). The primary arguments for vesicular release are the requirement for increases in cytosolic Ca^{2+} and for sensitivity to tetanus neurotoxin and bafilomycin. The major arguments for channel-mediated release are that several Cl_2 channel blockers reversibly inhibit release and that glutamate is not released in isolation but, rather, together with other amino acids present in high concentration in astrocytes, including taurine and aspartate (Kimelberg et al., 1990; Molchanova et al., 2007; Ye et al., 2003). Recently, unopposed gap junctions, called hemichannels, have been shown to release large amounts of glutamate and other amino acids in response to manipulation of extracellular [Ca^{2+}] (Ye et al., 2003). Likewise, activation of the P_2X_7 purine receptor results in glutamate release from cultured astrocytes (Duan et al., 2003).

Among various molecules released by astrocytes, below are some previously studied gliotransmitters: (a) excitatory and inhibitory amino acids (D-serine, glutamate, aspartate, GABA, glycine and taurine), (b) ATP and related nucleotides and nucleosides (purine nucleotides ATP), (c) eicosanoids and other lipid mediators (prostaglandins), (d) neuropeptides (proenkephalin, angiotensinogen, endothelins), (e) neurotrophins (nerve growth factor, neurotrophin-3, brain-derived neurotrophic factor), (f) cytokines (interleukins, interferons, tumor necrosis factor alpha), (g) structurally associated chemokines and (h) growth factors (Bergami et al. 2008; Bezzi and Volterra 2001; Blum et al. 2008; Fields and Stevens 2000; Fujita et al. 2009; Hussy et al. 2000; Kang et al. 2008; Liu et al. 2008; Medhora 2000; Sanzgiri et al. 1999; Snyder and Kim 2000).

Astrocytes utilize regulated exocytosis for the release of several gliotransmitters (Parpura et al., 2010; Parpura and Zorec, 2010). This process requires vesicles containing a chemical transmitter. Upon a merger of vesicular and plasma membranes, gliotransmitters stored in the vesicle lumen are secreted into the extracellular space. Astrocytes have vesicles which contain amino acids (e.g. glutamate and D-serine), peptides and nucleotides (e.g. ATP) as gliotransmitters. Amino acid glutamate is synthesized within astrocytes as a by-product of the tricarboxylic acid cycle (Hertz et al., 1999; Westergaard et al., 1996). D-serine is generated from L-serine by serine racemase, an enzyme found in astrocytes (Wolosker et al., 1999). ATP is produced via glycolysis and oxidative phosphorylation. ATP can mediate intracellular signalling by acting directly onto purinergic receptors.

2.1.2 Secretory vesicles

Astrocytes are now known to secrete a number of signalling molecules that participate in cell-to-cell communication, involving both neurons and glial cells. Of these signalling molecules, gliotransmitters such as ATP, glutamate, D-serine and neuropeptide Y (NPY), are well known. Vesicles that get engaged in regulated exocytosis are of many types (Gucek et al., 2012) which include small synaptic-like vesicles, larger dense-core vesicles and lysosomes (Hua et al., 2011; Jordan et al., 2005; Wienisch and Klingauf, 2006). In astrocytes several gliotransmitters are stored in secretory vesicles and are released in Ca^{2+}-dependent regulatory secretory pathway. Different types of vesicles in astrocytes are classified on the basis of their content or function (Tab. 1).

Table 1: Diameter of different vesicle types in astrocytes, values obtained from EM.

S. No.	Antibody	Diameter (nm)	Reference
1.	ANP	45 ± 2	(Potokar et al., 2008)
2.	VGLUT1	27 ± 12	(Bezzi et al., 2004)
3.	D-serine	39 ± 11	(Bergersen et al., 2012)
4.	BDNF	125 ± 22	(Bergami et al., 2008)
5.	LAMP1	155 – 560	(Brewer et al., 2004)
6.	Sb2	30 – 49	(Crippa et al., 2006)

In general, there are two types of secretory vesicles in astrocytes; translucent small synaptic-like vesicles and large dense-core vesicles.

Table 2: Compilation of vesicle sizes from different cell types.

S. No.	Type of vesicle	Antibodies used	Diameter (nm)	Method	Author
1.	Synaptic vesicles	-	40 & 46	EM	(Zhang et al., 1998)
2.	Synaptic vesicles	-	30 – 50	EM	(Qu et al., 2009)
3.	Synaptic vesicles	Theoretical	23 – 67	-	(Kim et al., 2000)
4.	Synaptic vesicles a) Hippocampal CA1 slice b) culture	- -	35 – 43 32 – 49	EM EM	(Hu et al., 2008)
5.	Synaptic vesicles	-	40 – 50	EM	(Dennison, 1971)
6.	Insulin vesicles	FM-dye	300	TEP	(Takahashi, 2007)
7.	Dense core vesicles a) NG 108-15 b) PC 12	- -	70 ± 17 106 ± 25	EM	(Cans et al., 2001)
8.	Synaptic vesicles (pineal glands)	Phosphotungstic acid	30 – 50	EM	(Jaim-Etcheverry and Zieher, 1969)
9.	Astrocytic vesicles	SV2	~40	EM	(Di Maio et al., 2011)
10.	Small clear & large dense core vesicles	AT2 receptor	100 – 1000	EM	(Coleman et al., 2009)
11.	Astrocytic vesicles	Sb2	30 – 49	EM	(Crippa et al., 2006)
12.	Astrocytic vesicles	BDNF	125 ± 22	EM	(Bergami et al., 2008)
13.	a) small clear synaptic vesicles b) large clear vesicles	- -	32 ± 6 70 ± 13	EM EM	(Rollenhagen et al., 2007)
14.	Electron dense vesicles DCVs	SERT	80 – 150	LM, EM	(Pickel and Chan, 1999)
15.	Small round clear vesicles	TH	40 – 60	LM, EM	(Pickel et al., 1989)
16.	Synaptic vesicles	VGLUT1 VGLUT2	28 ± 12 27 ± 9	TIRF TIRF	(Bezzi et al., 2004)
17.	SLMVs SVs	VGLUT1 D-serine	37 ± 11 40 ± 11	EM EM	(Bergersen et al., 2012)

Analogous to the neurotransmitters stored in synaptic vesicles of neurons, small signalling molecules of astrocytes are traditionally thought to be stored in small synaptic-like vesicles and released in a regulated fashion, which in turn participate in neuron-glial cell communication in the brain. However, the large dense core vesicles were also shown to contain a variety of small and large molecules that are of importance in cell-to-cell communication.

Several vesicles contain gliotransmitters (peptides, amino acids, ATP), membrane transporters, channels and other molecules (Halassa et al., 2007). In the context of studying exocytosis, it is essential to know the sizes of vesicles. The vesicle size is challenging to measure due to limitations in the methodology and microscopic techniques (fixation, accurate labelling, resolution limit). In the Tab. 2 we compiled the sizes for different vesicle types estimated with different microscopic techniques. With the super-resolution microscopic technique it is possible to determine the vesicle diameter more accurately. We compiled different antibodies and methods used for the size measurement of synaptic vesicles from the previous literature (Tab. 2). Tab. 2 shows the different values for different vesicle types estimated with different microscopic techniques. We tried to accurately measure these vesicle diameters with one of the super-resolution microscopic techniques. To study the single movement of a secretory vesicle, proteins involved in SNARE complex are the important mediator during exocytosis of these vesicles. We selected Sb2, one of the SNARE members typically present on the vesicle membrane in astrocytes.

2.2 SYNAPTOBREVIN

The exocytosis process was previously described by different mechanisms based on the characteristics of plasma membranes and transmitter release such as full fusion and kiss-run through transient fusion pore. It is assumed that the SNARE proteins present in the plasma membrane and vesicle membrane mediate the spatial specificity of the interaction between the vesicle and presynaptic membrane preceding fusion (Sollner et al., 1993). The studies have shown that the SNARE complex comprises two classes of components: (a) v-SNAREs, proteins present on the vesicles (predominantly Sb2; (Schoch et al., 2001)) and (b) t-SNAREs, proteins present on the target presynaptic plasma membrane (syntaxin and synaptosomal-associated proteins).

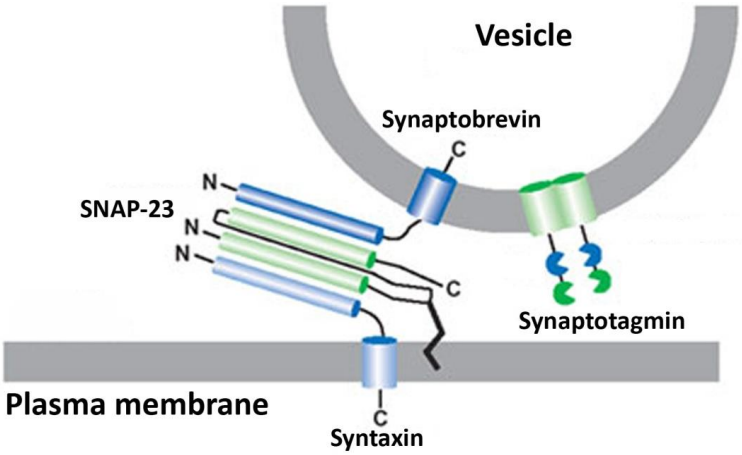

Figure 1: Pictorial view of the SNARE complex. The diagram shows the interactions between a v-SNARE; synaptobrevin on the astrocytic vesicle membrane and t-SNAREs; SNAP-23 and syntaxin, on the plasma membrane. These synaptic fusion proteins undergo priming reactions that allow them to form a four-helix bundle that is likely to pull the vesicle and plasma membranes together, overcoming the energetic barriers to fusion. (O'Connor and Lee, 2002)

The interaction between these two groups of proteins occurs through the highly conserved SNARE motifs present in these molecules that form a stable four helix bundle and bring together the vesicle and plasma membranes, thereby facilitating their fusion and release of the vesicle contents. Because of the characteristic complex formed by the three core proteins Sb2, syntaxin and SNAP-25 or 23 (in case of astrocytes), SNARE proteins are thought to catalyze the steps involved in the release by reducing the energy barrier (Li et al., 2007) and increasing the specificity of vesicle fusion as well as by directly facilitating pore formation by inducing distortion in the membranes.

SNARE proteins have been sequenced and their role in synaptic exocytosis or neurosecretion studied extensively (Bennett and Lowrie, 1992; Oyler et al., 1989; Trimble and Scheller, 1988). An important member of the SNARE family are Sb2 proteins of 19 kDa molecular mass that are integral to the vesicle membrane and are required for calcium-dependent vesicle fusion (Schoch et al., 2001). Sb2 facilitate pore formation by perturbing the vesicle membrane through their C-terminal transmembrane domains during SNARE "zippering" activity (Ngatchou et al., 2010). Sb2 are cleaved by Clostridium botulinum neurotoxin (BoNT) serotypes B, D, F and G, with each serotype specific for a given peptide bond, resulting in inhibition of exocytosis (Blasi et al., 1994). Deficiency of synaptobrevin impairs overall vesicular exocytosis and completely inhibits the calcium triggered portion of exocytosis (Schoch et al., 2001). Sb2 is a protein present on astrocytic or synaptic vesicles in rat brain (Crippa et al., 2006).

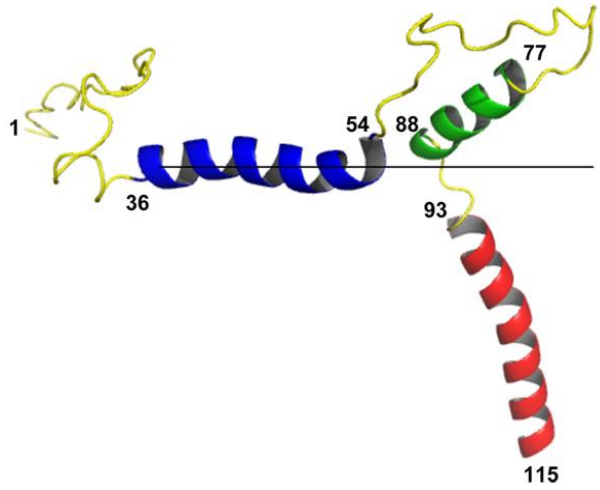

Figure 2: Structure of synaptobrevin2 (Sb2). The structure of Sb2 (1–116) in its lowest energy form in a dodecylphosphocholine micelles. This structure conforms well to the plane of a membrane, the interface of which is shown as a line. Helices I, II and III are colored in blue, green and red, respectively. (Ellena et al., 2009)

(Ellena et al., 2009) have found that in the SNARE complex, the SNARE motif of Sb2 forms a 55-residue helix, but it has been assumed to be mostly unstructured in its prefusion form. NMR data of full-length Sb2 in dodecylphosphocholine (DPC) micelles reveals two transient helical segments flanked by natively disordered regions and a third more stable helix. In Fig. 2, the transient helix I comprise the most N-terminal part of the SNARE motif, transient helix II extends the SNARE motif into the juxtamembrane region and the more stable helix III is the transmembrane domain. These helices may have important consequences for SNARE complex folding and fusion: helix I likely forms a nucleation site, the C-terminal disordered SNARE motif may act as a folding arrest signal and helix II likely couples SNARE complex folding and fusion (Ellena et al., 2009).

2.2.1 SynaptopHluorin

It is a genetically encoded optical indicator of vesicle release and recycling. It consists of a pH-sensitive form of GFP fused to the luminal side of a vesicle membrane protein Sb2. It is used to study neurotransmitter release through plasma membrane. (Miesenbock et al., 1998) has used the superecliptic green synaptopHluorin (GSpH), as functional readout for monitoring the fusion pore following the merger between vesicle and plasma membranes.

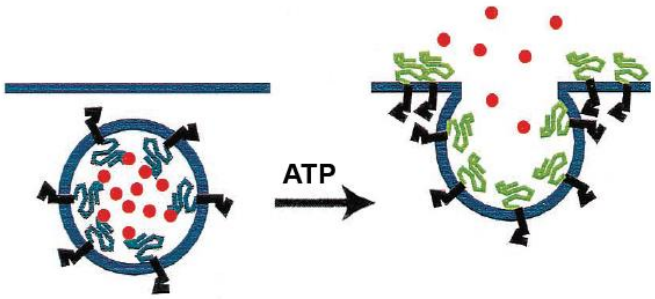

Figure 3: Exocytosis relieves the proton-dependent quenching of ecliptic-pHluorin fluorescence. The pHluorin molecule (blue) is attached to the luminal aspect of Sb2 (black). At the resting pH of ~5.5 within vesicles, the fluorescence signal from pHluorin is quenched. The red dot denotes the H^+. On the addition of ATP, the vesicles undergo fusion with the plasma membrane leading to the externalization of pHluorin to pH of ~7.3. This relieves the proton-dependent quenching (green) and causes an increase in fluorescence (Sankaranarayanan et al., 2000).

In acidic environment pHluorin is non-fluorescent and becomes fluorescent upon alkalization of vesicle lumen (Fig. 3), as the fusion pore is established and the protons leave the vesicle lumen through it (Balaji and Ryan, 2007; Bowser and Khakh, 2007; Budzinski et al., 2011; Miesenbock et al., 1998; Miesenbock, 2012). The pHluorin is the only probe available to signal the activity of genetically specified synapses in intact neural tissue (Miesenbock, 2012). Based on known amino acids contributing to the chromophore pockets of the GFP vs. enhanced YFP (Miyawaki et al., 1997; Nagai et al., 2002), Parpura et al. introduced mutations to GSpH to generate its yellow shifted emission variant (Fig. 4).

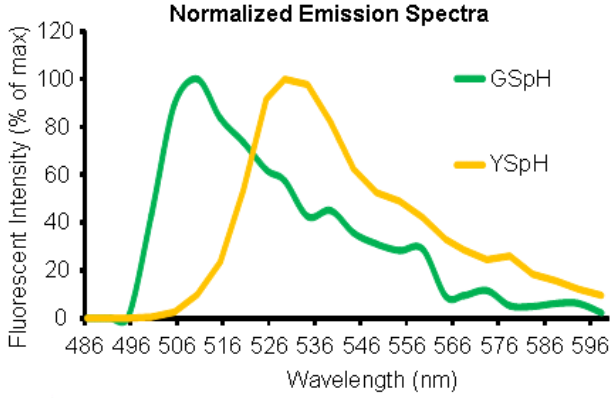

Figure 4: Emission spectra of synaptopHluorins. Spectrum in green shown is GSpH having λ_{em} at 510 nm and spectrum in yellow shown is YSpH having λ_{em} at 530 nm. The increase in the emission wavelength by 20 nm directly influences the YSpH fluorescence (figure courtesy of Prof. Dr. Vladimir Parpura).

2.3 CONFOCAL LASER SCANNING MICROSCOPY (CLSM)

Confocal microscopy is a fluorescence technique used mainly to observe cells marked with fluorescent dyes. The principle of confocal laser scanning microscopy was first described by Marvin Minsky in 1957. It is a commonly used technique due to its ability to reject out-of-focus light. The break-through of confocal microscope over conventional microscope is due to a pinhole. As a result, the detector can only detect light that has passed the pinhole (Pawley and Masters, 1996). With a confocal and its variable pinhole it is therefore possible to exclusively image a thin optical slice out of a thick specimen, known as optical sectioning. Depending on the pinhole diameter, the data and computation methods for resolution and depth discrimination is different. The bigger the pinhole, the more photons get through it, but also the less discrimination against scattered light from outside the focal volume. A pinhole smaller than 1 Airy Unit (A.U.) does not improve resolution, it just loses light. Therefore, a pinhole 1 A.U. seems to be a good compromise.

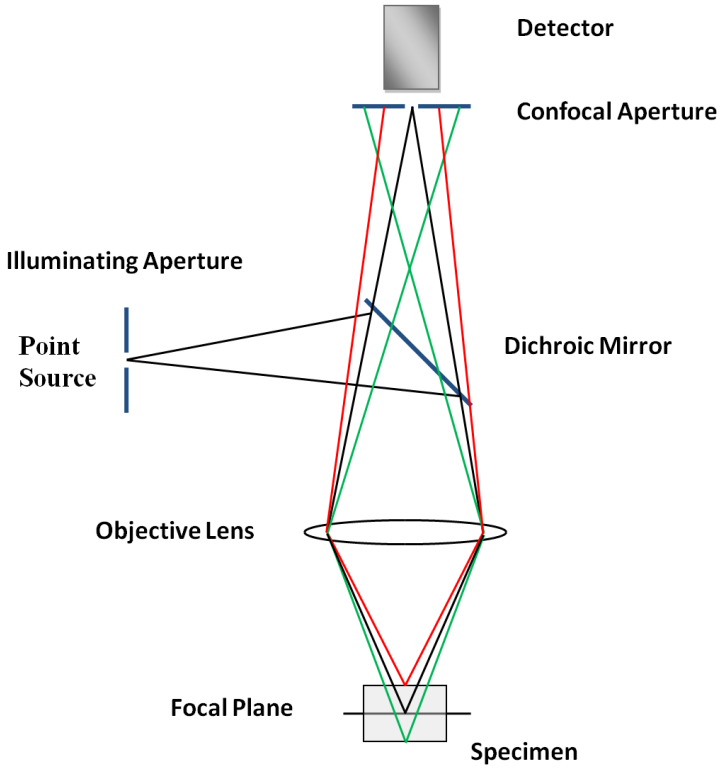

Figure 5: Schematic representation of the optical path in confocal laser scanning microscope. The entrance point source, focal plane in the specimen and confocal aperture (pinhole) are the main confocal features. The line shown in black is the only signal that reaches the detector. A dichroic mirror reflects the illuminating beam which passed focal plane and was reflected by the mirror on which the specimen is lying. Only the reflected beam that passes focal plane focuses onto the pinhole and reaches the detector (Pawley and Masters, 1996).

An objective lens is used to focus a laser beam onto the specimen, where it excites fluorescence as shown in Fig. 5. The fluorescent radiation is collected by the objective and efficiently directed onto the detector via a dichroic beam splitter. The range of wavelength of the fluorescence spectrum is selected by an emission filter, which also acts as a barrier, blocking the excitation laser line. The pinhole is arranged in front of the detector, on a plane conjugate to the focal plane of the objective lens. Light coming from planes above or below the focal plane is out of focus when it hits the pinhole, so most of it cannot pass the pinhole and therefore does not contribute to forming the image. The pinhole suppresses stray light which further improves image contrast. Hence, this microscopy is widely used in neuroscience research. The resolving power in the CLSM depends only on the wavelength of the illumination light, rather than exclusively on the emission wavelength as in the conventional microscope. Compared to the conventional fluorescence microscope, CLSM with large pinhole diameters leads to a gain in resolution by the factor ($\lambda_{em}/\lambda_{ex}$) via stokes shift.

2.3.1 Diffraction limit

Significant amount of our knowledge regarding the structure of biological organelles and their processes at the cellular and subcellular level has come from the ability to visualize them by microscopic techniques. Among various microscopic techniques, fluorescence microscopy is one of the most widely used techniques in glial research because of its two principal advantages: (i) specific cellular components may be observed through molecule-specific labelling and (ii) light microscopy allows the observation of structures inside a live sample in real-time (Wilson, 2011b). The most common technique, CLSM with its ability to image the in-focus image by the use of a pinhole has become a standard approach for imaging of live biological specimens (Wilson, 2011a). It has been used to study morphology and different cell organelles of neurons (Fusco et al., 2004) as well as astrocytes (Bergami et al., 2008; Kacem et al., 1998).

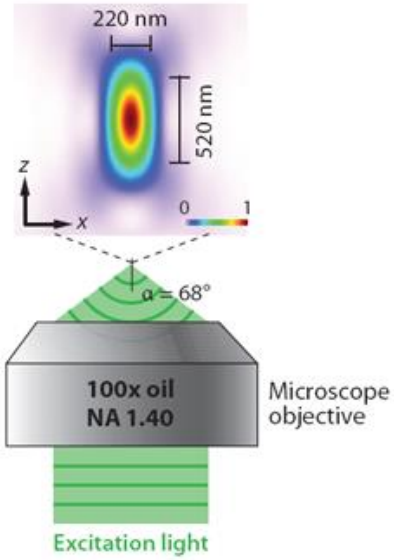

Figure 6: Diffraction limit in confocal microscope. The point spread function of a point source, visualized through an oil immersion objective with numerical aperture (NA) = 1.40 the wavelength of the excitation light is 550 nm and a medium has a refractive index η = 1.515. The intensity distribution in the *x*-*z* plane of the focus spot is computed numerically and shown in the upper panel and the full width at half-maximum in the lateral and axial directions are 220 nm and 520 nm, respectively (Huang et al., 2009).

However, limitation of this technique is the resolution limit, determined in 1873 (Abbe, 1873) meaning it is difficult to study the properties of cell organelles, which have dimensions below the limit of optical resolution. This limit is known as diffraction limit. The resolution limit of a microscope in lateral direction is given by $d \approx \lambda/2NA$ where, λ is the wavelength of the excitation light and NA is the numerical aperture of the objective defined as $NA = \eta \sin\alpha$, with η being the refractive index of the medium and α being the half-cone angle of the focused light produced by the objective. For example, if we considered wavelength of light as 543 nm and numerical aperture of oil immersion objective is 1.40 (Fig. 6). Then, PSF is ~200 nm in lateral direction (*xy* plane) and ~500 nm in axial direction (*z* plane) which is larger than any subcellular structures of a cell. Over estimation due to diffraction limit can be overcome by super-resolution microscopies (Huang et al., 2009) which possess better lateral and axial resolution. There are several super-resolution microscopies such as, a nonlinear effects to sharpen a PSF of the microscope; structured illumination microscopy (SIM) (Schermelleh et al., 2008) and stimulated emission depletion (STED) (Wildanger et al., 2009), other technique based on localization of individual fluorescent molecules; photoactivated localization microscopy (PALM) (Hess et al., 2006) and stochastic optical reconstruction microscopy (STORM) (Rust et al., 2006).

2.4 SUPER-RESOLUTION MICROSCOPY

2.4.1 Structured illumination microscopy (SIM)

An approach to increase the spatial resolution of optical microscopy is to apply a patterned illumination field to the sample. In this approach, the spatial frequencies of the illumination pattern mix with those of the sample features, shifting higher frequency features to the lower frequencies that are detectable by the microscope (Gustafsson, 2000). The periodically modulated illumination light patterns are used to generate sub diffraction limit images of the specimen. A sinusoidal illumination pattern is applied to a fluorescent sample which results in interference pattern with the features present in a sample.

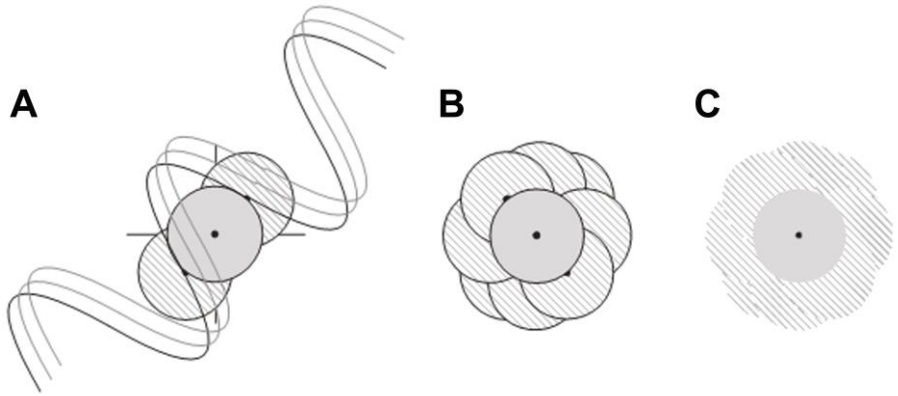

Figure 7: Concept of resolution enhancement by structured illumination microscopy. The grey circle at the centre of each panels show the 'observable region' of a conventional microscope. (**A**) A sinusoidally illumination pattern has only three Fourier components which are shown by three black dots. The possible positions of the two side components are limited by the same circle that defines the observable region. If the sample is illuminated with structured light, moiré fringes will appear which represent information that has changed position in reciprocal space. The amounts of that movement correspond to the three Fourier components of the illumination. The observable region will thus contain, in addition to the normal information two other offset regions. (**B**) With a sequence of observable region and two offset regions with different orientation and phase of the pattern, it is possible to recover information from an area twice the size of the normally observable region, corresponding to twice the normal resolution. (**C**) Theoretical increase in the 'observable region' in case of SIM.

The diffraction-limited fringes of this interference pattern called Moiré fringes, which contain information about the underlying structural pattern of the sample that cannot be observed by CLSM. SIM is one of the super-resolution microscopy which increases the resolution twice compared to the CLSM (Gustafsson, 2000; Huang et al., 2009). By applying a set of illumination patterns of different spacing and rotational angles to the specimen (Fig. 7), sub-diffraction limited structural information can be extracted from

Fourier transforms of the resulting interference patterns (RodrĂ-guez et al., 2009). This technique relies on the mathematical calculations to convert raw data into final images. Structured illumination extends optical resolution since spatial frequencies beyond the classical cut-off frequency are brought into the passband of the optical microscope by frequency mixing (Gustafsson, 2000; Gustafsson et al., 2008). Considering all these features of SIM, one can use this technique for routine measurements of live cells. We used this microscopy for the vesicle diameter measurements and nano-architectural analysis of a Sb2 protein present on the secretory vesicles in astrocytes.

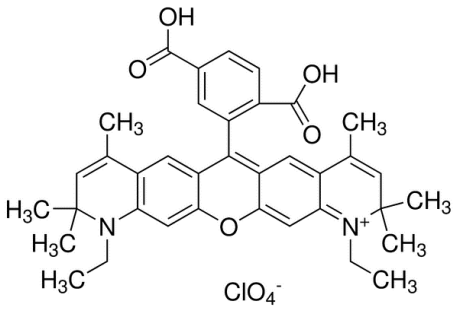

Figure 8: Structure of Atto 594 dye. Atto dye has following properties - longest wavelength absorption maximum, λ_{abs} = 601 nm; molar extinction coefficient at the longest-wavelength absorption maximum, ε_{max} = $1.2x10^5$ $M^{-1}cm^{-1}$; emission maximum wavelength, λ_{em} = 627 nm; fluorescence quantum yield, η_{fl} = 85 %; Fluorescence decay time, τ_{fl} = 3.5 ns.

To obtain the best resolution of a microscope we need an optimum fluorescent dye. Atto fluorescent dyes are designed for high sensitivity applications, including single-molecule detection. Atto dyes have rigid structures that do not show any cis-trans isomerization. Thus, these dyes display exceptional intensity with minimal spectral shift on conjugation. Atto dyes have been used in previous studies because of its three main features; intense brightness, high photostability and long fluorescence lifetime (Fernandez-Suarez and Ting, 2008). We selected Atto 594 (Fig. 8) depending on the following properties: (a) high fluorescence yield (b) high photostability (c) excellent water solubility (d) very little aggregation (e) the laser source is compatible of this dye.

3 MATERIALS AND METHODS

3.1 CELL CULTURE

Cortical astrocytes were isolated from 2-3 days old rats and maintained as described (Schwartz and Wilson, 1992). Briefly, until confluence astrocytes were maintained in the growth medium (Dulbecco's modified eagle medium (DMEM, high glucose content: 4500 mg/L) supplemented with 10% fetal bovine serum (FBS), 1 mM sodium pyruvate, 2 mM L-glutamine and 25 μg/ml penicillin-streptomycin antibiotics), in 95% air and 5% CO_2 at 37 °C. Confluent cultures were shaken overnight three times. Following third shaking, cells were trypsinized and cultured further. For experiments astrocytes were plated on 1% poly-L-lysine coated 22 mm glass coverslips and supplemented with growth medium. Unless stated otherwise, all the chemicals were obtained from Merck (Darmstadt, Germany) and Sigma (Diesenhofen, Germany). The care for experimental animals was in accordance with International Guiding Principles for Biomedical Research Involving Animals developed by the Council for International Organizations of Medical Sciences and Directive on Conditions for issue of License for Animal Experiments for Scientific Research Purposes (Official Gazette of RS, 40/85 and 22/87).

3.2 PLASMID DNA

Plasmid DNA (pDNA) encoding genetically modified Sb2 was prepared in Prof. V. Parpura's laboratory (Department of Neurobiology, Center for Glial Biology in Medicine, University of Alabama, Birmingham, Alabama, USA). We used three different pDNAs: (a) YSpH (Sb2 with YpH fused to the luminal end) (details in Fig. I), (b) mCherry-YSpH YSpH with mCherry on the cytoplasmic N-terminus and (c) YSpH-7aa-mCherry plasmid has both fluorescent proteins (YpH and mCherry) at the C-terminus of Sb2. mCherry is appended to the C-terminus of YSpH by the polypeptide linker (L) containing 7 amino acid residues (SGLRSRA). The last two constructs are expressed under the control of the cytomegalovirus (CMV) promoter.

3.3 ISOLATION OF PLASMID DNA

YSpH, mCherry-YSpH and YSpH-7aa-mCherry encoding Sb2 protein were amplified and purified by PureYield™ Plasmid Miniprep System according to manufacturer's instructions (Promega).

3.4 TRANSFECTION OF ASTROCYTES

Astrocytes were transfected with 1-2 μg of pDNA (Gandhi and Stevens, 2003; Miesenbock et al., 1998) using FuGene 6 transfecting reagent, according to the manufacturer's instructions (Roche, Mannheim, Germany). 3% UltroserG (Life Technologies) was added after incubation period of 3 h at 37 °C and then cells were incubated overnight. The transfected astrocytes were used for experiments at least 24 h after transfection.

3.5 IMMUNOCYTOCHEMISTRY

3.5.1 Labelling of different vesicle types

The cells were washed with phosphate buffered saline (PBS; Sigma-Aldrich, ZDA) fixed with 4% paraformaldehyde (PFA; Thermo Scientific, USA) in PBS for 15 min and incubated in 0.1% Triton X-100 (Sigma-Aldrich) for 10 min at room temperature. Nonspecific background staining was reduced by blocking buffer, containing 3% bovine serum albumin (BSA; Sigma-Aldrich) and 10% goat serum in PBS (37 °C, 1 h). The cells were stained sequentially with primary antibodies, diluted in 3% BSA in PBS and incubated for 2 h at 37 °C or overnight at 4 °C. The cells were then rinsed in PBS and stained with secondary antibodies at 37 °C for 45 min. Finally, the cells were mounted on glass slides using SlowFade Gold antifade reagent (Invitrogen, Eugene, OR). Vesicles were labelled with rabbit polyclonal antibodies to VGLUT1 (1:800; Synaptic Systems), ANP (1:800; Abcam), BDNF (1:2000; Abcam) and D-serine (1:1000; Gemacbio). Secondary antibodies against rabbit IgG conjugated to fluorescent dye Atto 594 (1:100; Sigma Aldrich) were used.

3.5.2 Labelling of Sb2 vesicles for measuring the distance between fluorophores

YSpH transfected astrocytes were washed with PBS fixed in 4% PFA in PBS for 15 min and incubated in 0.1% Triton X-100 for 10 min at room temperature. Nonspecific background staining was reduced by blocking buffer, containing 3% BSA and 10% goat serum in PBS (37 °C, 1 h). We used anti-Sb2 mouse polyclonal primary antibody against a synthetic peptide corresponding to amino acids 1-18 of synaptobrevin2 (Sb2 1:500; Abcam, Cat. No. ab3347). Astrocytes were incubated with anti-Sb2 antibody diluted in 3% BSA in PBS for 2 h at 37 °C or overnight at 4 °C. The cells were then rinsed in PBS and stained with secondary antibodies against mouse IgG conjugated to fluorescent dye Atto 594 (1:100; Sigma Aldrich) at 37 °C for 45 min. The cells were then again rinsed four times with PBS and finally, mounted on glass slides using SlowFade Gold antifade reagent (Invitrogen, Eugene, OR). To stain vesicle lumen for measurement of vesicle diameter,

YSpH transfected astrocytes were incubated with 100 nM LysoTracker Red DND-99 (Molecular Probes) at 37 °C for 5 min.

3.6 OPTICAL IMAGING

3.6.1 Confocal laser scanning microscopy (CLSM)

Cells were examined with an inverted Zeiss LSM 510 META confocal microscope (Germany) equipped with 63x/1.4 Oil DIC objective, He/Ne laser and argon laser. YSpH was excited by 488 nm line of argon laser and Atto were excited by 543 nm line of He/Ne laser. The emission light for 488 and 543 was collected through band pass filter 505-530 nm and 545-560 nm, respectively.

3.6.2 Structured illumination microscopy (SIM)

Cells were imaged by Zeiss ELYRA PS.1 super-resolution microscope (Germany) equipped with five different grating frequencies for SIM for optimal matching of illumination pattern to laser wavelength and objective lens. The cells were scanned using Plan-Apochromat 63x/1.4 Oil DIC M27 objective and HBO X-Cite 120 lamp. Cells were excited with laser lines (561 and 488 nm). 16-bit depth images were acquired with an EMCCD camera (Andor iXon 885) with variable exposure. The standard beads used in intensity analysis have diameter 200 nm (Zeiss, Germany).

3.7 SINGLE VESICLE PHLUORIN EXPERIMENTS

Astrocytes expressing YSpH were scanned using LSM 510 META confocal microscope. The cells were kept in 200 µl of extracellular solution (ECS) for live imaging, consisting of (in mM) 130 NaCl, 5 KCl, 2 $CaCl_2$, 1 $MgCl_2$, 10 D-glucose, 10 HEPES, pH 7.2 and ~300 mOsm/L. To increase the free concentration of calcium ions [Ca^{2+}] in cytoplasm, astrocytes were stimulated with 100 µM ATP prepared in ECS. To induce intracellular alkalization of vesicles, extracellular solution containing 45 mM NH_4Cl was used. Time-lapse image series of 200 frames (1 frame/s) were acquired. During acquisition, we applied ATP and NH_4Cl solutions at 30 s and 120 s time points, respectively.

3.8 PHOTO BLEACHING EXPERIMENTS

Astrocytes expressing YSpH were scanned using an LSM 510 META confocal microscope. The cells were kept in 200 µL ECS. Extracellular solution containing 45 mM NH_4Cl was used for the vesicle alkalization. A time-lapse imaging series of 300 frames (1

frame/s) were acquired. During acquisition, we applied NH_4Cl at 10 s and increased the laser power by factor of 2-3 after 50 s.

3.9 DATA ANALYSIS

3.9.1 Colocalization of fluorophores

To quantitatively analyse large collections of images, we used the ColocAna software (Celica, Slovenia). The automated analysis enables uniform, objective analysis of all images regardless of their appearance. This enables statistical analysis of degree of colocalization between different markers (Kreft et al., 2004). In this colocalization analysis, we determined the optimal threshold value to be 51 a.u., which corresponds to 20% of maximal brightness level of image. In our experiments, the degree of colocalization is calculated as the percentage of green fluorescent pixels versus the total fluorescent puncta in an image.

3.9.2 Distance and diameter measurements

The measurements of the distance between the two fluorophores were performed in ZEN software by drawing a line profile over two neighbouring fluorophores, Atto-YpH, mCherry-YpH and two Atto peaks (Fig. 13*D*). Then the distance between the peaks of respective fluorophores was measured. To measure the diameter of astrocytic vesicles, we measured full width at half maximum (FWHM) values of the equatorial fluorescence intensity line profile of LysoTracker stained vesicle (Balaji and Ryan, 2007). For better precision we measured the diameter of each vesicle in *x* and *y* directions.

3.9.3 Data fitting

The Gaussian curve fitting on frequency distributions was performed in OriginLab software by using Levenberg-Marquadt X^2 minimization for nonlinear least-square fitting. The intensity analysis of pHluorin experiments was done with ImageJ 1.35j software (National Institute of Health, USA) by selecting square region of interests (ROIs = 1.33 x 1.33 μm^2) which are overlaid on each fluorescent punctum and thereby, mean intensities were estimated using intensity vs. time monitor plugin. We fitted the Gaussian curves by using Levenberg-Marquardt X^2 minimization fit parameter and the equation for the Gaussian fitting is, Counts/Bin = $\{A/[\sigma(\sqrt{2\pi})]\}$*exp $\{-[(x-\mu)^2/2\sigma^2]\}$ where, A = area under the curve, σ = sigma (half of FWHM), μ = mean of the distribution and x = variable present on x axis which differs in different experiments.

3.9.4 Statistical significance

The values for the Gaussian fit are given in mean ± s.e.m. Statistical significance of the data was tested in SigmaPlot (Student t-test and ANOVA). The significance level was checked at the $P < 0.05$.

4 RESULTS

4.1 VESICLE DIAMETER OF DIFFERENT VESICLE TYPES IN ASTROCYTES

The important step to resolve the exact architecture of a vesicle is to measure its diameter. In astrocytes there are different types of vesicles. We labelled them with different antibodies to mark glutamatergic, peptidergic and purinergic vesicles (Tab. 2). We focused on vesicles that transport atrial natriuretic protein (ANP), brain-derived neurotrophic factor (BDNF), D-serine and vesicular glutamate transporter 1 (VGLUT1). The immunocytochemical labelling was performed with anti-ANP, anti-BDNF, anti-D-serine and anti-VGLUT1 antibodies, followed by anti-rabbit IgG Atto 594 secondary antibody.

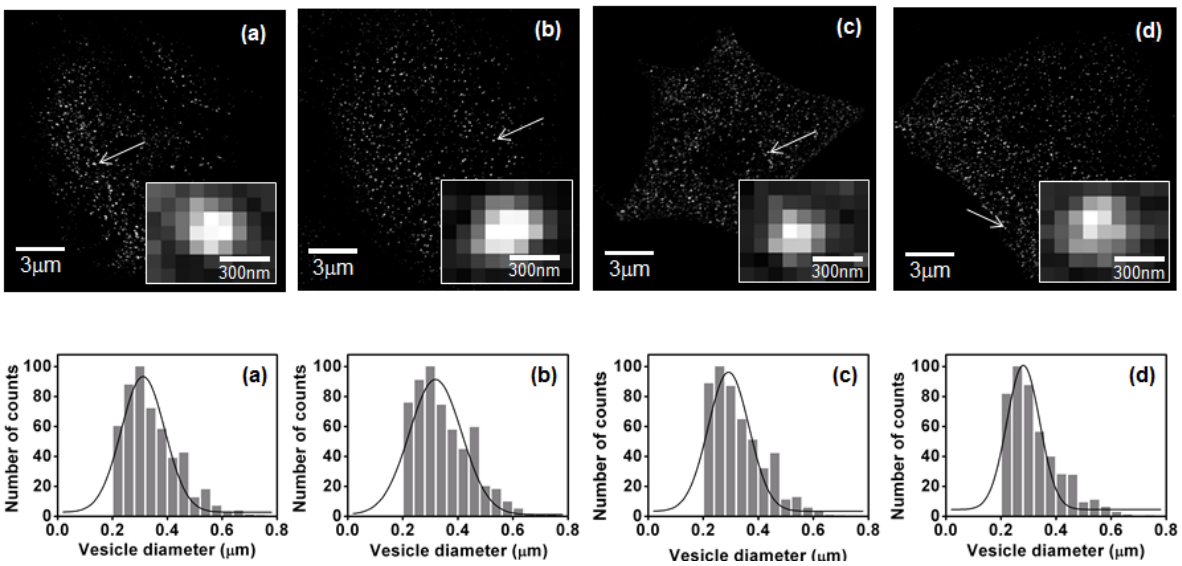

Figure 9: CLSM images of astrocytes with marked different vesicle types. Top panel shows the astrocytic vesicles marked with (**a**) anti-ANP (**b**) anti-BDNF (**c**) anti-D-serine (**d**) anti-VGLUT1. Insets show enlarged fluorescent puncta with the pixel size 140 nm. Bottom panel shows the respective frequency distribution plots for the vesicles marked with different antibodies in astrocytes. The values for the Gaussian fits (mean ± s.e.m.) are tabulated in Tab. 3.

We approached the measurement of vesicle diameters by comparing the two fluorescence microscopic techniques. Fig. 9 and Fig. 10 show the images acquired from CLSM and SIM, respectively, for the astrocytes labelled with the above mentioned antibodies. We clearly noticed the diffraction limit of ~200 nm in case of CLSM. According to the literature, the vesicles likely have diameters smaller than 200 nm, but the resolution of confocal microscope limits the further resolution. Therefore, we measured the diameter for the same vesicle types with SIM.

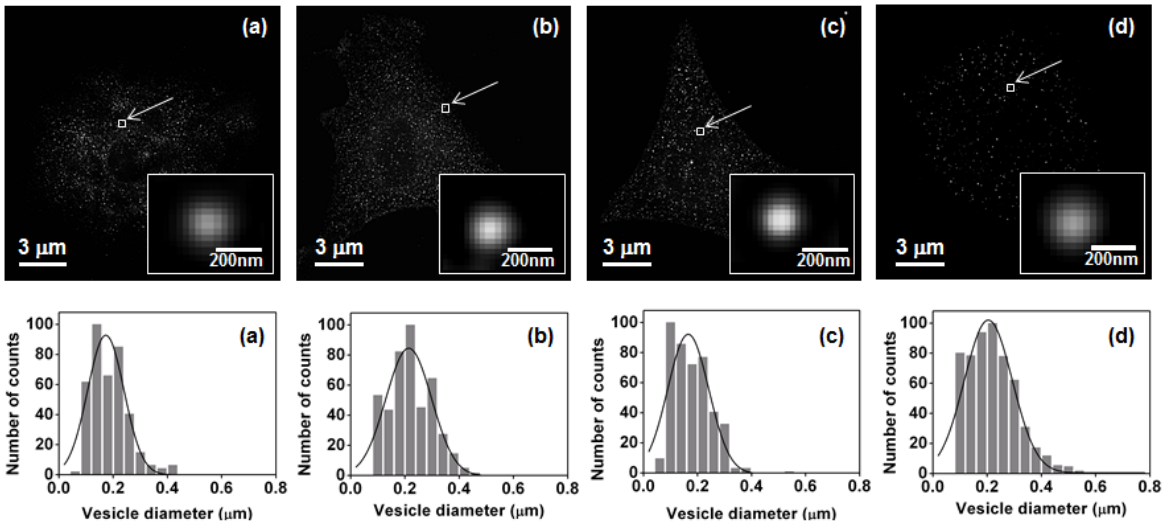

Figure 10: SIM images of astrocytes with marked different vesicle types. Top panel shows the astrocytic vesicles marked with (**a**) anti-ANP (**b**) anti-BDNF (**c**) anti-D-serine (**d**) anti-VGLUT1. Insets show enlarged fluorescent puncta with the pixel size 40 nm. Bottom panel shows the respective frequency distribution plots for the vesicles marked with different antibodies in astrocytes. The values for the Gaussian fits (mean ± s.e.m.) are tabulated in Tab. 3.

The frequency distribution plots obtained in the case of SIM are not limited at 200 nm but at ~100 nm, which agrees well with the theoretical limit of the SIM (Gustafsson, 2000). By fitting the Gaussian curves on the diameter distribution of different vesicle types, we determined the mean values (mean ± s.e.m.) that are represented in Tab. 3.

Table 3: Diameter of different vesicle types, values estimated from CLSM and SIM.

Vesicle type	**Diameter (nm) (mean ± s.e.m.)**	
	CLSM	SIM
ANP	311 ± 8	176 ± 5
BDNF	319 ± 11	212 ± 8
D-serine	292 ± 9	168 ± 9
VGLUT1	281 ± 7	203 ± 7

By measuring the diameter of different vesicle types in astrocytes, we found that the size differs irrespective of the vesicle content. The diameter of ANP and D-serine containing vesicles are smaller than BDNF and VGLUT1 vesicles. The comparison of these vesicle

types with a conventional confocal and a super-resolution microscopy describe that by using a super-resolution microscopy one can measure vesicle diameters, which are closer to the values determined by electron microscopy.

To study the mechanism of secretory vesicles which is governed by SNARE complex formation it is important to know the location of Sb2 in different types of vesicles in astrocytes. Therefore it is important to know whether atrial natriuretic protein, brain-derived neurotrophic factor, D-serine and vesicular glutamate transporter 1 are present in the same compartment as Sb2 in the secretory vesicles. We transfected astrocytes with YSpH (pHluorin protein tagged with Sb2) followed by immunolabelling with the same antibodies as for vesicle diameter measurements (anti-ANP, anti-BDNF, anti-D-serine and anti-VGLUT1). This data describes the relation between the secretory vesicles and different peptidergic and glutamatergic vesicles present in astrocytes. We observed from the experiments that the colocalization between Sb2 and other vesicle types are <20%. This suggests that not all the peptidergic and glutamatergic vesicles are directly involved in SNARE-dependent exocytosis. They may transfer their contents to the vesicle having Sb2 and present in the active zone or close to the plasma membrane for the gliotransmitter release.

4.2 ARRANGEMENT OF SYNAPTOBREVIN ON A SINGLE VESICLE IN ASTROCYTES

To understand the processes in a cell and their mechanisms in detail, we alsoneed to know the arrangement of every protein present in a cell. We focused on vesicle associated membrane protein, secretory vesicles and their fusion mechanism with the plasma membrane in astrocytes. To describe the architecture of Sb2 proteins on a single vesicle at the nanometer scale, we used a genetically modified construct with pHluorin protein in the vesicle lumen, attached to the C-terminal of Sb2. The other end (N-terminal) of the same protein was marked with antibodies, conjugated with a dye, which can be excited with different wavelength (compared to the pHluorin). By considering the length of Sb2 protein, the size of fluorophores attached to it and average size of antibodies (Ellena et al., 2009; Lehninger, 1975; Rizzo et al., 2009b; Stryer, 1995; Sutton et al., 1998), we drawn a detailed schematic of astrocytic vesicle (Fig. 11) in which a modified construct of Sb2 is expressed, with a pHluorin moiety in the vesicle lumen (labelled with A) while the same vesicle is exposed to immunolabelling with antibodies against the cytoplasmic domains of Sb2 (labelled with B). The schematic was drawn by considering the Sb2 in its lowest energy form (Ellena et al., 2009). As Sb2 tends to dimerize (Laage and Langosch, 1997) and can also arrange in different ways on the vesicle surface. Therefore, different possible

orientations of the protein may reflect different values of the measured distance between the two fluorophores.

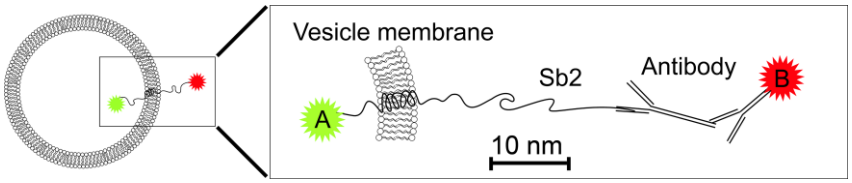

Figure 11: Schematic representation of a vesicle-associated membrane protein (Sb2) fluorescently labelled at the luminal and cytoplasmic sides of the vesicle membrane. The diagram represents an astrocytic vesicle (left) in which a modified version of Sb2 is expressed, with a pHluorin moiety in the vesicle lumen (Fluorophore A) and with immunolabelled cytoplasmic domains (Fluorophore B). The boxed diagram on the right shows a detailed architecture of Sb2 across the vesicle membrane. This diagram is drawn to the scale, by considering the length of Sb2 (Lehninger, 1975; Stryer, 1995).

We first performed the experiments with multi-spectral beads (the average diameter reported by Zeiss, Germany was 200 nm) and we performed the channel alignment for red and green fluorescent puncta on the image. This automatic channel alignment is used to correct the linear lateral (*x*, *y*) and axial (*z*) drifts, rotational offsets in the image plane in *x* and *y* as well as a first order stretching in the image plane in *x* and *y*. The line profile on these aligned puncta of beads has shown the overlapped Gaussian fits, meaning that respective channels are perfectly aligned. Moreover, we have observed that the direction vectors of the YpH and Atto fluorophores shifts in vesicles does not display any pattern, which would indicate chromatic shifts (e.g. radially to the center of the field of view).

To measure the distance between adjacent fluorescent tags we first performed colocalization experiments of two adjacent proteins (Shroff et al., 2007). Thus we introduced pHluorin in the vesicles by transfecting astrocytes and immunolabelled them with antibodies against the cytosolic domain of Sb2 therefore, we marked a transmembrane protein across the vesicle membrane. To measure the distance between these two adjacent fluorophores we used CLSM but, with its resolution limit of 200 nm, one will see maximum colocalization and therefore, we also scanned the same samples on super-resolution microscopy (i.e., SIM). The astrocytes were transfected with plasmids encoding YSpH; green fluorophores. The vesicles labelled with primary antibodies against Sb2 followed by secondary antibodies Atto 594 goat anti-mouse IgG; red fluorophores.

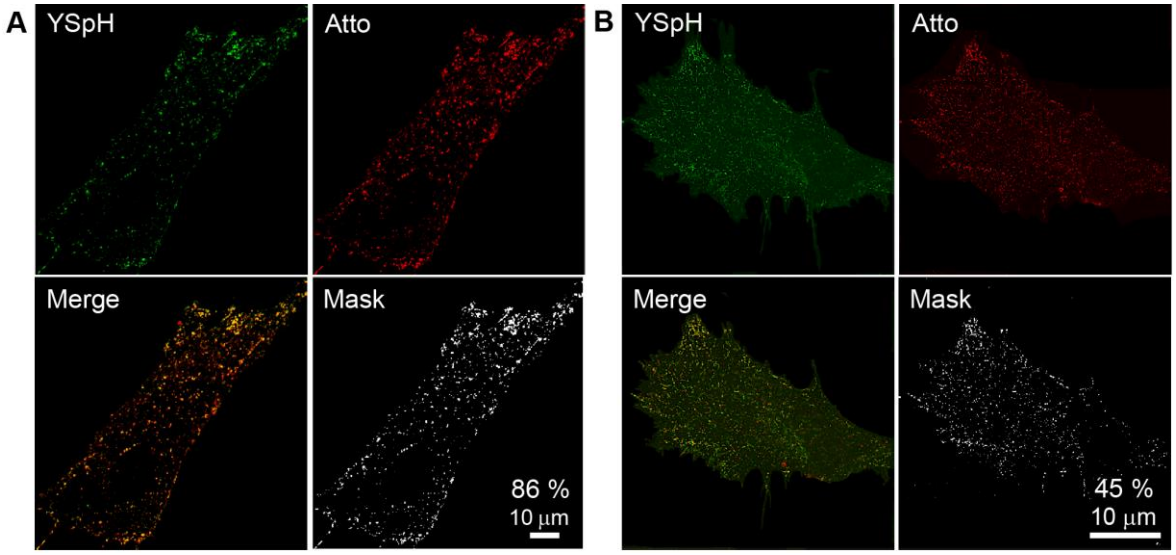

Figure 12: Comparison of images of cultured rat astrocytes with fluorescently labelled Sb2 at the vesicle lumen and cytoplasmic sites obtained by CLSM and SIM. (**A**) and (**B**) are the images from CLSM and SIM, respectively. To stain Sb2 in the vesicle lumen, astrocytes were transfected with a Sb2 clone with a pHluorin moiety (YpH; green). To stain Sb2 domains on the cytosolic side of the vesicle membrane, we immunolabelled cells with a primary antibody against Sb2 and with the secondary antibody Atto 594 goat anti-mouse IgG (Atto; red). Merge panels show the overlay of the fluorescence of YpH and Atto arising from vesicle lumen and cytoplasmic sites. The degree of colocalization (%) between YpH and Atto in a cell is expressed vs. pixels representing all YSpH-vesicles was 86% and 45% with CLSM and SIM, respectively. The mean of colocalization (mean ± s.e.m.) analysed by CLSM and SIM is 83 ± 2% (n = 20) and 40 ± 4% (n = 9), respectively, significantly different ($P < 0.001$). The reduced level of colocalization obtained with SIM is consistent with the higher resolution of this method vs. CLSM.

We calculated the degree of colocalization (%) between YpH and Atto as the extent of all colocalized pixels in the cell versus pixels representing YpH. The percentage of colocalization analysed from five different astrocytes by CLSM and SIM is 83 ± 2% and 40 ± 4%, respectively. There is a statistical significant difference between the percentage of colocalization analysed from CLSM and SIM images (P = 0.002, Student's t-test). The panel in bottom right corner of Fig. 12A and 12B shows mask of these colocalized pixels. The difference in the percentage of colocalization of YpH and Atto with these two microscopies is due to the superior resolution of SIM, compared to CLSM (Gustafsson, 2000). Hence, we found that YpH and Atto fluorophores are present in close proximity, a few nanometers from each other (Shroff et al., 2007).

We have also calculated the theoretical degree of colocalization based on the point spread function of fluorophores with the predicted resolution limit of each microscopic method (200 nm for CLSM and 120 nm for SIM) and by assuming that fluorophores are 65 nm apart. The theoretical degree of colocalization for CLSM and SIM at given distance is

62.4% and 28.5%, respectively (green (YpH) and red (Atto) vs. pixels representing all green pixels). The difference in the measured and theoretical degree of colocalization can be attributed to the fact that the real resolution limit is in fact slightly worse than the predicted one.

We proceeded further with colocalization analysis by measuring the distance between fluorophores in SIM images. We analysed individual pairs of YpH and Atto by measuring the distance between two different fluorescent tags of a single protein. Based on the orientation of fluorescent molecules we observed morphologically different patterns of Sb2 attachment to the vesicle membrane (Fig. 13).

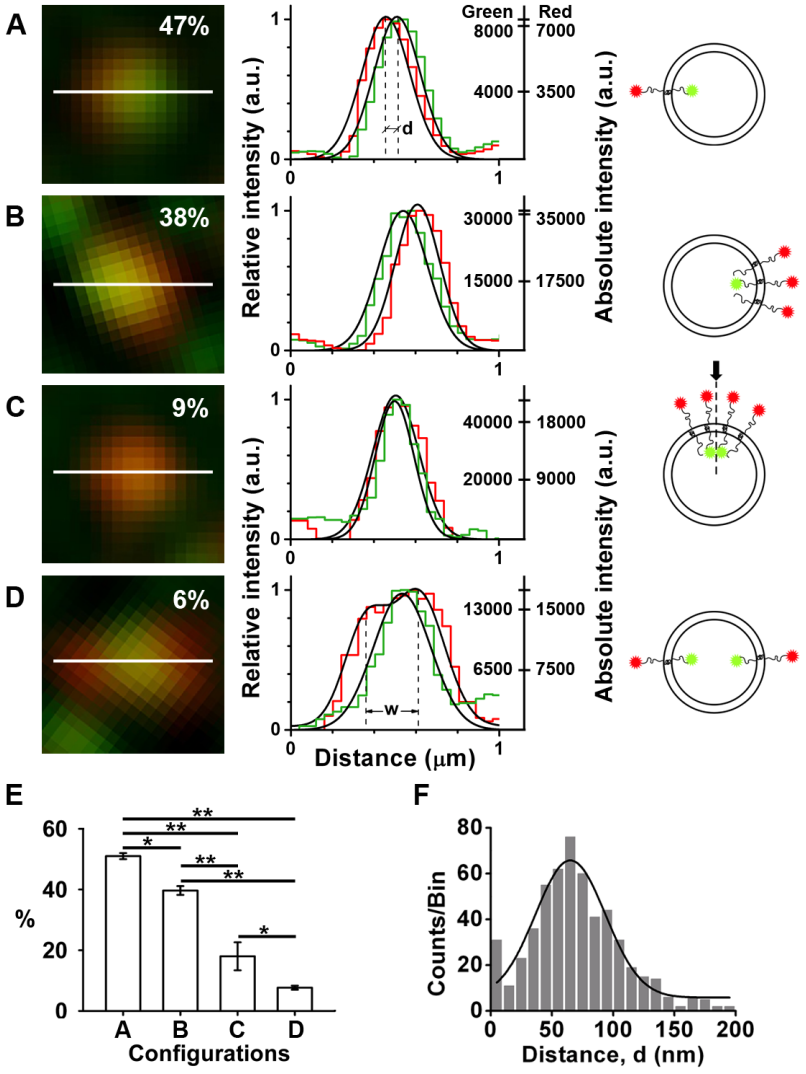

Figure 13: Patterns of two Sb2-associated fluorophores, YpH and Atto, reveal nonuniform vesicular distribution of Sb2. There are three separate images positioned horizontally in each panel (**A-D**). First, SIM images which show different arrangements of Atto (red) and YpH (green) fluorophores labelling vesicle

associated membrane protein. The image in the middle represents the frequency distribution of normalized fluorescence intensity (red and green fluorescence), estimated by dividing intensities with the maximum value and obtained along the line in the left image for both fluorophores. The image on the right shows the possible arrangements of two fluorophores in a single vesicle. The order of the images is according to their abundance of configurations observed and their percentage of abundance in a particular astrocyte is shown on the SIM image itself. (**E**) The histograms for the abundance of pairs. We analysed 3 astrocytes in which a total of 349 vesicles were examined from different experiments and in these we have observed configuration of type A: 44 ± 2%; type B: 34 ± 2%; type C: 15 ± 3%; type D: 7 ± 1%). '$*P < 0.02$' and '$**P < 0.001$'. As indicated in line profile of panel (**A**), the distance (proximity) between the green and red fluorophores 'd' can be determined. The frequency distribution plot for the distance measured from each pair of YpH and Atto tagged fluorophores shown in panel (**F**). The distance was measured by plotting normalized fluorescence intensity histograms along the line on the image. The mean value for distance between YSpH and Atto is 65 ± 2 nm (mean ± s.e.m.), which is calculated by fitting a Gaussian curve on the frequency distribution plot of the form: $\text{Counts/Bin} = \{A/[\sigma(\sqrt{2\pi})]\}*\exp\{-[(\text{Distance(nm)}-\mu)^2/2\sigma^2]\}$ where, total counts $A = (3102 \pm 161)$; $\sigma = 32$; $\mu = (65 \pm 2)$ nm. The squared correlation coefficient was $R^2 = 0.95$, $n = 325$ which is significantly different than zero ($P < 0.001$).

We analysed the average intensity of fluorophores to identify the possible number of molecules in each pattern. We checked the line profile for each of these arrangements and found that there are typically four different types of configurations observed on the surface of the vesicle membrane. In Fig. 13 these types are shown in accordance to their abundance in different astrocytes (A: 44 ± 2%; B: 34 ± 2%; C: 15 ± 3%; D: 7 ± 1%). The most common configuration shown in panel A has one unit of each YpH and Atto. The configuration shown in panel B is the second frequent arrangement of Sb2 across the vesicle membrane present in astrocytes, in this case red fluorophores are present in one direction and therefore they seem to be clustered.

If a fluorophore is used to tag two or more entities, then the interaction between these fluorophores is masked by the properties of fluorescence emission and this can be analysed quantitatively (Zinchuk and Grossenbacher-Zinchuk, 2009). The clustering of protein molecules are known as nano-aggregate molecules (Shroff et al., 2007; Willig et al., 2006). The presence of Atto clusters on the surface of vesicle membrane may be due to the polarization effect from YSpH present in the vesicle lumen. We have drawn respective models for each type to visualize the exact pattern of YpH and Atto arrangement on a vesicle. These models were drawn depending on their intensity profile and considering the number of protein molecules in each fluorophore. Fig. 13E describes the statistical significance for the abundance of these pairs. As indicated in line profile of panel A, the distance was measured between the peaks of Gaussian curve fitted on the intensity of green and red fluorophores which is designated as 'd'. The frequency distribution plot for the distance measured from each pair of YSpH and Atto tagged fluorophores shown in Fig. 13F. This distance was measured by plotting normalized fluorescence intensity histograms along a line on the image (Wildanger et al., 2009).

Table 4: The average (± s.e.m.) of absolute intensities obtained by fitting Gaussian curves on green (YpH) and red (Atto) fluorescent puncta.

Type	YpH (mean ± s.e.m.)	Atto (mean ± s.e.m.)	Number of vesicles
A	11306 ± 177	15892 ± 371	153
B	11655 ± 72	37944 ± 2371	119
C	27663 ± 1671	36719 ± 2084	54
D	12531 ± 218	24759 ± 50	23

We fitted a Gaussian curve on the frequency distribution histograms to determine the mean distance between YpH and Atto and obtained a value of 65 ± 2 nm (mean ± s.e.m.), n = 325. In Fig. 13D 'w' is the distance between the peaks of two red fluorophores, which describes the diameter of a vesicle because these red fluorophores are antibodies against Sb2 protein and they always present on the cytoplasmic domain of the protein i.e., present on the surface of vesicle membrane. Hence, with type D one can measure the diameter of a vesicle in astrocytes and the average vesicle diameter in these cases is 260 ± 15 nm. To measure the diameter of a vesicle one can pervade its lumen and to confirm the sizes obtained from 'w', we filled the lumen of astrocytic vesicles. Fig. I shows the two constructs, mCherry-YSpH and YSpH-7aa-mCherry which are used for the estimation of length of Sb2 present on a single vesicle in astrocytes. We performed the colocalization study for genetically modified Sb2 so as to confirm the estimation of length between Atto and YpH. Therefore, we used mCherry-YSpH and YSpH-7aa-mCherry (details in Annexes).

We measured the distance between mCherry and YpH fluorophores by drawing a line intensity profiles on these pairs. We obtained the distance of 57 ± 1 nm in case of mCherry-YSpH construct and the distance in case of YSpH-7aa-mCherry was <10 nm; this is because fluorophores are only seven amino acids apart.

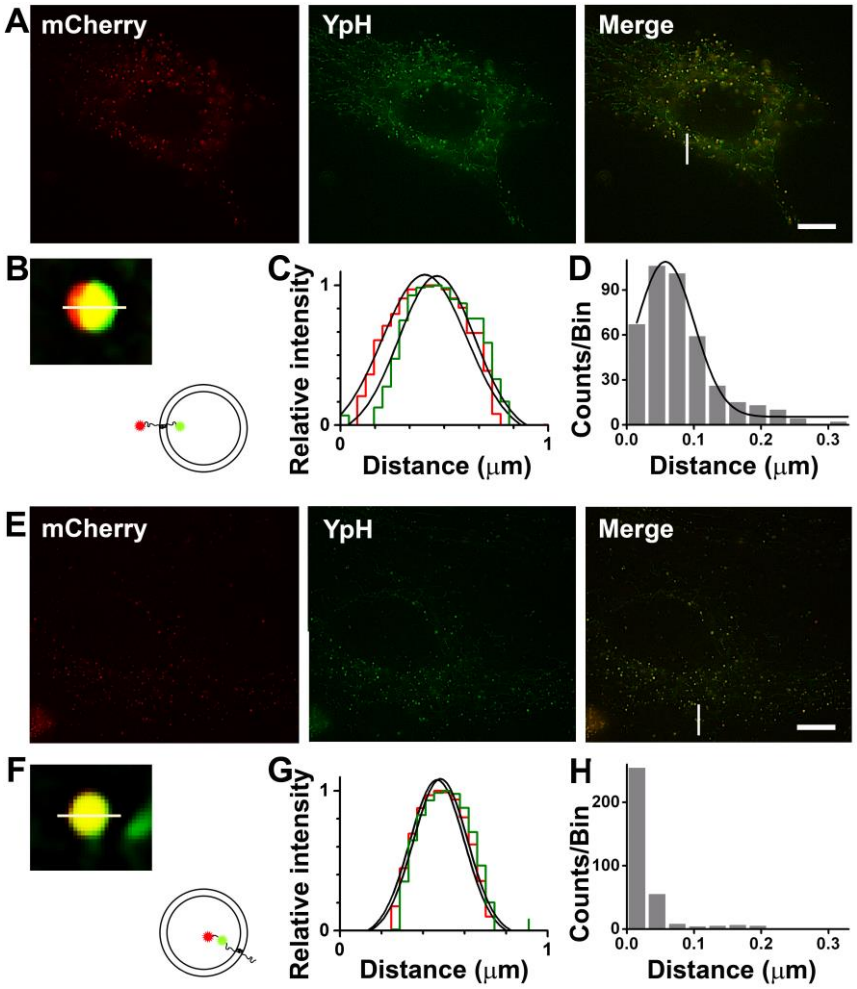

Figure 14: SIM images reveal the distance between two fluorophores. (**A**) and (**E**) are the SIM images showing astrocytes transfected with mCherry-YSpH and YSpH-7aa-mCherry plasmids, respectively. Scale bar: 10 μm. Merge panels show the overlay of the fluorescence of YpH (green) and mCherry (red) signals. (**B**) and (**F**) are the mCherry and YpH pair enlarged from the image. (**C**) and (**G**) are the intensity profiles of lines drawn on these pairs. The histograms (**D**) and (**H**) are frequency distribution plots for the distance between two fluorophores. (**D**) In case of mCherry-YSpH, the mean value for distance between YSpH and mCherry is 57 ± 1 nm (mean ± s.e.m.), which is calculated by fitting a Gaussian curve on the frequency distribution plot with the form: Counts/Bin = {A/[$\sigma(\sqrt{2\pi})$]}*exp{-[(Distance(nm)-μ)^2/2σ^2]} where, total counts A = (11089 ± 611); σ = 43; μ = (57 ± 1) nm. The squared correlation coefficient was R^2 = 0.98, n = 403 vesicles, 7 cells, significantly different than zero (P < 0.001).

4.3 DIAMETER MEASUREMENTS OF PHLUORIN-LADEN VESICLES IN ASTROCYTES

We selected LysoTracker Red DND-99 to stain the vesicle lumen of astrocytes in live conditions. LysoTracker stains all the acidic compartments present in a cell (Potokar et al., 2010) but, in this experiment one need to ensure that measured diameter are only from

vesicles and no other acidic compartments of astrocytes. Therefore, before labelling the vesicle lumen with LysoTracker we transfected astrocytes with YSpH to confirm that the measured diameter are from vesicles only (Fig. 15). Hence, an estimation of diameter was done only with the vesicles expressing YSpH.

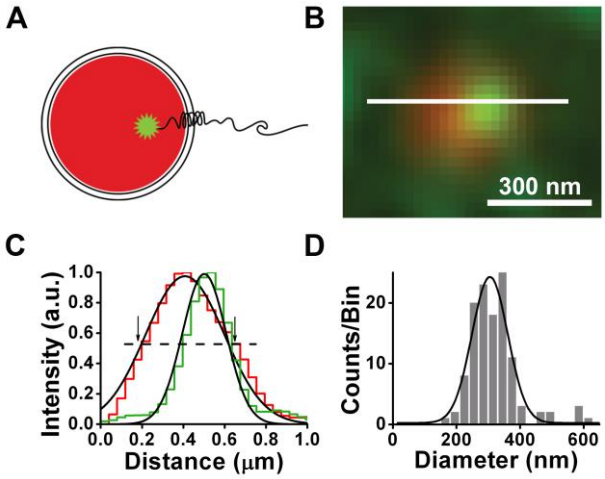

Figure 15: Measurement of vesicle diameter in live astrocytes by SIM. (**A**) Diagram of an astrocytic vesicle loaded with LysoTracker DND-99 (red), expressing YSpH (green) and (**B**) corresponding SIM image in live astrocyte. A line profile drawn in panel (**B**) shows in (**C**) the intensity and the location of LysoTracker and pHluorin protein in the vesicle lumen. The dashed-line indicates how the apparent diameter of the vesicle was determined; by measuring the full width of the Gaussian curve of the red fluorophore at half maximum intensity (FWHM) of the graph. Note the intersection with the Gaussian curve drawn on the normalized intensity of the red fluorophore, marked with arrows. (**D**) The frequency distribution plot for the apparent vesicle diameter, determined as defined in panel (**C**). The mean value (mean ± s.e.m.) of the apparent vesicle diameter is 305 ± 4 nm (n = 8 cells, 119 vesicles), calculated by fitting a Gaussian curve of the form: $\text{Counts/Bin} = \{A/[\sigma(\sqrt{2\pi})]\} * \exp\{-[(\text{Diameter(nm)}-\mu)^2/2\sigma^2]\}$ where, total counts A = (3466 ± 220); σ = 57; μ = (305 ± 4) nm. The squared correlation coefficient was R^2 = 0.92 (n = 119), significantly different than zero (P < 0.001).

The Gaussian curve profile shown in Fig. 15C is from the fluorescence intensity line profile, drawn on a vesicle (Fig. 15B). The dashed-line with two arrows indicates how the apparent diameters of astrocytic vesicles were determined; by measuring the full width of the Gaussian curve of the red fluorophore (Atto) at half maximum intensity (FWHM). Fig. 15D is the frequency plot for the distribution of diameter, determined as defined in panel C. The mean value (mean ± s.e.m.) of the apparent vesicle diameters is 305 ± 4 nm (n = 8 cells, 119 vesicles). The number of vesicles per astrocyte was lower because it is essential that a pH of a vesicle is relatively high (Fig. I) to see the fluorescence of YSpH, while LysoTracker labels predominantely acidic compartments.

4.4 ANALYSIS OF FLUORESCENCE INTENSITY OF ATTO AND YPH FLUOROPHORES

We estimated the diameter and intensity of standard beads by SIM for comparison with that of astrocytic vesicles. The diameter was calculated as stated in the previous chapter in *x* and *y* directions. Fig. 16A shows a fluorescent punctum of the standard beads from a SIM image. The line profiles across the punctum shows FWHM of 250 nm (Fig. 16B), which is the diameter of individual bead. Fig. 16C, the frequency distribution of fluorescent bead diameters with a mean value 254.8 ± 0.3 nm (mean ± s.e.m.).

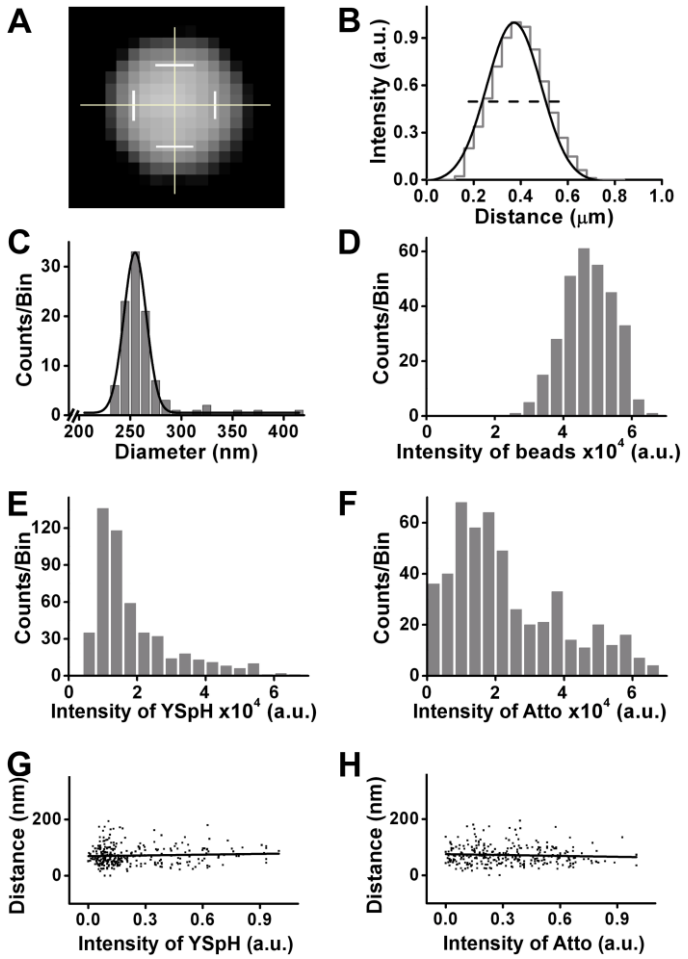

Figure 16: Fluorophore intensity distributions indicate multiples of Sb2 molecules per vesicle. (**A**) SIM image shows a fluorescent punctum of the standard bead. (**B**) The line profiles across the punctum show FWHM of 250 nm, the diameter of individual bead. (**C**) Frequency distribution of fluorescent bead diameters with a mean value 254.8 ± 0.3 nm (mean ± s.e.m.), was determined by fitting by a Gaussian curve of the form: Counts/Bin = $\{A/[\sigma(\sqrt{2\pi})]\}$*exp{-[(Diameter(nm)-$\mu$)^2/2$\sigma^2$]} where, total counts A = (921 ± 23); σ = 11; μ = (254.8 ± 0.3) nm; R^2 = 0.99 (n = 100). (**D**) The fluorescence intensity distribution of fluorescent beads. Frequency distribution plots of YSpH intensities (**E**) and Atto fluorophores (**F**) as recorded on Fig. 13. The

intensity of each pair was measured separately from three cells in different experiments (n = 300 vesicles). (**G**) and (**H**) Scatter plots of the distance between YpH and Atto with their respective intensities. Lines represent regression lines of the form: Distance (nm) = (9.0 ± 8.7)*Intensity (a.u.) + (69.6 ± 2.8) for YpH and Distance (nm) = (-10.5 ± 8.7)*Intensity (a.u.) + (75.2 ± 3.5) for Atto. The slopes of lines are not different from zero (P_{YpH} = 0.303 and P_{Atto} = 0.224, ANOVA).

The frequency plots of fluorescence intensity of beads (Fig. 16D) and fluorophores tagged with Sb2 (YpH, Fig. 16E; Atto, Fig. 16F) showed that Atto has a broader distribution of intensities. The intensity for each pair Atto-YpH was measured separately from three cells in different experiments (n = 300 vesicles). A comparison of these intensity distributions with standard beads suggests that there is more than one Sb2 molecule present on the vesicle membrane.

We also checked whether the intensity of fluorophore is related to the distance between the fluorophores present on a single vesicle. Scatter plots of the distance between YpH and Atto with their respective intensities shown in Fig. 16G and 16H, respectively. These plots show that there is no correlation between the intensity of individual fluorophore and the distance between them. After this quantitative indication of proteins, the further step was to design single-molecule experiment for estimation of the number of Sb2. In YSpH transfected astrocytes that were immunolabelled by anti-Sb2 antibody conjugated with Atto dye, we did not observe a correlation between the fluorescence intensity and the area of the Atto fluorescent puncta (Fig. 17).

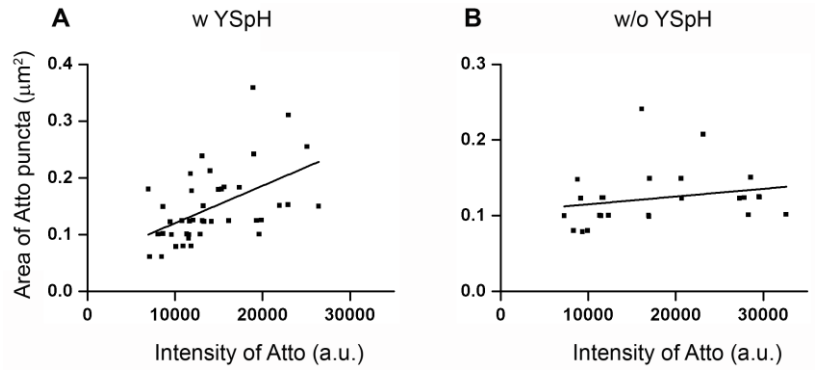

Figure 17. Correlation between fluorescence intensity and area of the Atto punctum. (**A**) and (**B**) are the panels for Atto punctum with YSpH and without YSpH, respectively. The scatter plot between area of Atto puncta and fluorescence intensity shows no correlation, with squared correlation coefficients (R^2) of 0.24 (P < 0.001) and 0.01 (P = 0.275) in case of panels (**A)** and (**B)**, respectively.

4.5 YSPH EXPRESSION AND THE NUMBER OF SB2 MOLECULES ON SINGLE VESICLES IN LIVE ASTROCYTES

We observed three types of fluorescent evokes of pHluorin after stimulation (Fig. 18B). First, an increase in intensity only after the application of NH_4Cl solution and this is a typical example for intensity failure after ATP stimulation and this type is prominent. Second, an increase in intensity after application of ATP solution (after 30 s) and the intensity remain constant till the addition of NH_4Cl solution (after 120 s) in extracellular medium. Third, an increase in intensity after addition of ATP solution but, drop down after one minute and shoot up after the addition of NH_4Cl solution.

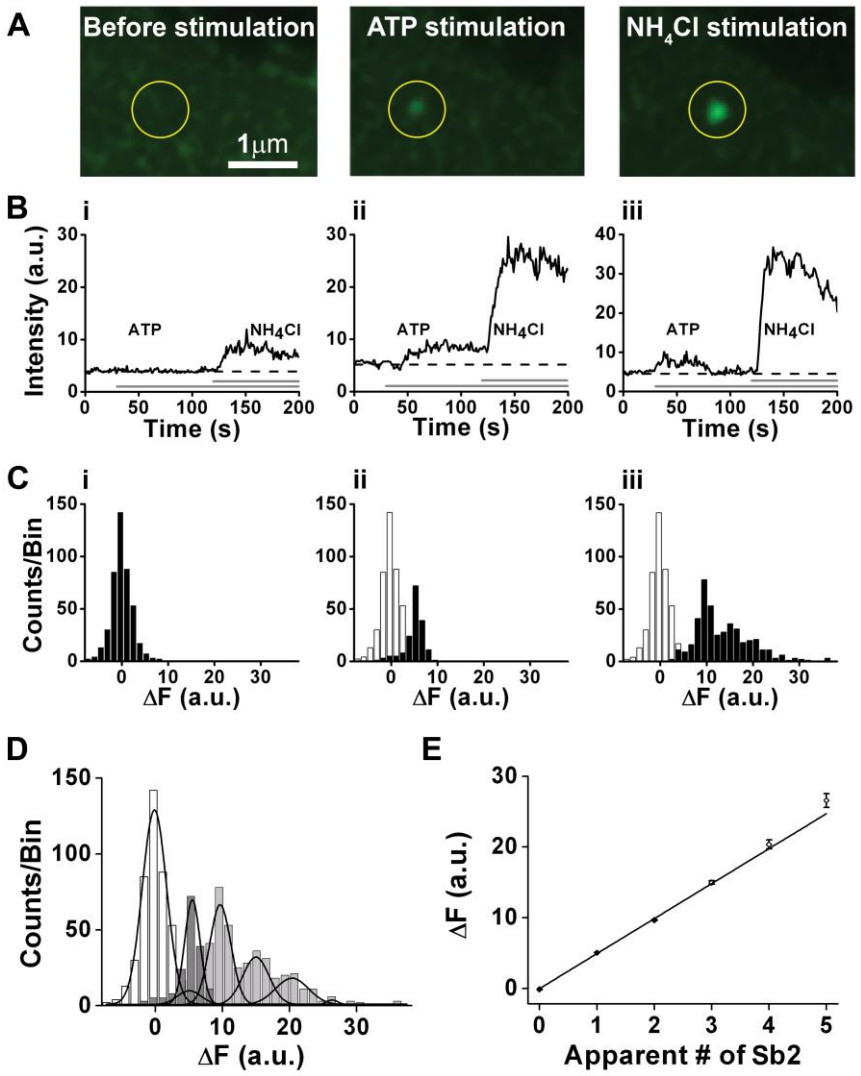

Figure 18: Stimulation of YSpH-labelled vesicles by ATP and NH_4Cl reveals the number of Sb2 molecules present on a single astrocytic vesicle. (**A**) Time series frames of a representative YSpH positive vesicle recorded by confocal microscopy. A subsequent increase in the fluorescence intensity before and

following successive stimulations with ATP and NH_4Cl was recorded [For the details see Supplementary Information (SI) Fig. S1]. (**B**) Different examples of the time-dependent changes in fluorescence intensity of individual vesicles: Left; ATP failed to evoke increase fluorescence intensity, however NH_4Cl elicited an increase. Middle; ATP application elicited a sustained increase in fluorescence intensity that was augmented after NH_4Cl. Right; ATP elicited a transient increase in fluorescence intensity. (**C**) Amplitude distributions of fluorescence intensity of the background trace, recorded in nine astrocytes before and after stimulations (R^2 = 0.99; n = 1045). In this panel, 1st amplitude plot is for the background; 2nd plot shows amplitude in black, recorded after ATP application and the amplitude in white same as before; 3rd plot shows amplitude recorded after NH_4Cl. (**D**) Combined plot for the baseline and intensities after ATP (dark grey) and NH_4Cl (light grey) stimulations. The Gaussian curves are fitted by using Levenberg-Marquardt minimization fit keeping standard deviation as determined in the background shown in panel (**C)** and the equation of the form, Counts/Bin = $\{A/[\sigma(\sqrt{2\pi})]\}$*exp$\{-[(\Delta F-\mu)^2/2\sigma^2]\}$. The values of A (area under the curve) and μ (mean value of the peak) for these Gaussian fits are given in Table 5. (**E**) The peak position Gaussian fit for different modes of intensities is obtained as a fit parameter of the form: Change in fluorescence, ΔF (a.u.) = (4.95 ± 0.040)*Apparent # of Sb2 + (-0.02 ± 0.05) where, # = number or multiples of Sb2 molecule. The squared correlation coefficient was R^2 = 0.997 (n = 1045), significantly different than zero (P < 0.001).

We plotted the distribution of background fluorescence intensities of nine astrocytes (n = 1045 events) which had the mean value of the change in fluorescence (ΔF) around zero arbitrary unit. To this distribution we fitted a Gaussian curve using Levenberg-Marquardt minimization fit parameter with baseline offset (y_0) near to zero. The same parameter was used to fit another Gaussian curve on the amplitude distribution obtained after stimulation with ATP solution. The average of standard deviation (σ) from background and ATP fluorescence which is equals to 1.5 a.u. This σ value is used to fit multiple Gaussian curves in case of multimodal amplitude distribution obtained after stimulation with NH_4Cl solution (Fig. 18C). The combined plot for the baseline and intensities after ATP (dark grey) and NH_4Cl (light grey) stimulations. The Gaussian curves are fitted by using Levenberg-Marquardt minimization fit keeping standard deviation as determined in the background shown in Fig. 18C and the equation of the form, Counts/Bin (a.u.) = $\{A/[\sigma(\sqrt{2\pi})]\}$*exp$\{-[(\Delta F\ (a.u.)-\mu)^2/2\sigma^2]\}$. The values of area under the curve, sigma (σ) and mean of the peak (μ) for these Gaussian fits are tabulated in Table 5. In all these fits, baseline offset $y_0 \approx 0$ as we observed all the Gaussian curves have the value of y_0 close to zero.

The Gaussian curves fitted on distribution of intensity amplitudes recorded before and after stimulations is shown in Fig. 18D. The respective value in the table gives an insight in the number of fluorescent puncta present on vesicle membrane. First mode corresponds to the background and the modes after 1st mode likely denote the possible number of molecules. The peak after ATP stimulation in Fig. 18C shows that there is only one molecule which gets fluorescent after the application of physiological stimulus. This difference in intensities after different stimulations suggests that after ATP addition, the fluorescent Sb2 molecules may be present locally to the membrane fusion site and that the fusion pore may

hinder the further alkalization of vesicle lumen. As NH_4Cl is used for saturated alkalinity, it increases the pH of all the contents in lumen. The linear fit shown in Fig. 18E is plotted between the change in fluorescence (ΔF) and the modal values obtained from Gaussian fit (i.e., apparent # of Sb2). The peak position in Gaussian fit of different modes of fluorescence intensities is obtained as a fit parameter of the form: ΔF (a.u.) = (4.95 ± 0.04)*Apparent # of Sb2 + (-0.02 ± 0.05) where, # represents the number or the multiples of Sb2 molecule. The squared correlation coefficient was R^2 = 0.997 (n = 1045), significantly different than zero ($P < 0.001$). Hence, this confirms that there are maximum five YSpH molecules present on the surface of a vesicle membrane in astrocytes.

Table 5: Stimulation experiment: Area under the curve (A) and mean value of each peak (μ) obtained from Gaussian curves by using Levenberg-Marquardt minimization fit with $y_0 \approx 0$.

Gaussian fits		***A*** **(mean ± s.e.m.)**	**Sigma (*σ*)**	***μ*** **(mean ± s.e.m.)**
Background		581.55 ± 18.48	1.79	-0.14 ± 0.06
ATP		199.65 ± 6.28	1.12	5.51 ± 0.04
NH_4Cl	1st	41.72 ± 12.77	1.61	5.05 ± 0.50
	2nd	262.56 ± 15.12	1.37	9.66 ± 0.06
	3rd	154.16 ± 30.75	1.78	14.98 ± 0.25
	4th	108.39 ± 30.02	2.34	20.37 ± 0.63
	5th	9.22 ± 4.69	0.35	26.75 ± 0.94

It should be noted that inherent to our experimental design, here we could only interrogate those vesicles that undergo kiss and run with stable-pore formation of varying duration (see below), but not the full fusions, where the vesicle collapses into the plasma membrane. The intensity patterns after application of ATP or NH_4Cl were found to be different, indicating that the addition of ATP makes visible only some YSpH molecules due to dequenching mediated by partial and/or by restricted alkalization of the vesicle lumen after opening of the narrow fusion pore. This is an intriguing finding as it may point out to an unappreciated mechanism for pH buffering of vesicular lumen and it should be explored in the near future. Indeed, these measurements were limited to kiss-and-run events as full fusion would cause dissipation of YSpH signal in the plasma membrane as vesicular membrane collapses to and dilutes its content within the plasma membrane.

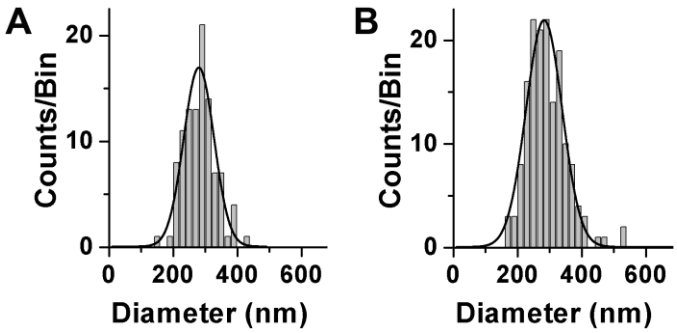

Figure 19: Diameters of astrocytic vesicles expressing YSpH after ATP and NH_4Cl stimulations. The Gaussian fit over the frequency distribution plot have the peak value (mean ± s.e.m.); (**A**) 280 ± 3 nm (*n* = 101) in case of ATP stimulation and (**B**) 282 ± 3 nm (*n* = 156) in case of NH_4Cl stimulation.

Additionally, we measured the vesicle diameter of astrocytes expressing YSpH from the same stimulation experiments. To measure the diameter we selected the frames at 40 s and 130 s for ATP and NH_4Cl stimulations, respectively. The mean values for the apparent vesicle diameter distribution are 280 ± 3 nm and 282 ± 3 nm (P = 0.45, Mann-Whitney Test) in case of ATP and NH_4Cl stimulation, respectively (Fig. 19). This proves that the vesicles expressing YSpH after respective stimulations are single vesicles and that the increase in fluorescence is not the consequence of vesicle clusters.

4.6 PHOTO BLEACHING OF YPH FLUOROPHORES AUTHENTICATE THE NUMBER OF SB2 MOLECULES IN LIVE ASTROCYTES

To confirm the number of Sb2 molecules we also performed the bleaching experiments. We transfected the astrocytes with YSpH and performed the experiments on live astrocytes. We followed a simple procedure for these experiments; the recordings were taken by stimulating the transfected astrocytes with the same concentration of NH_4Cl solution as used in ATP stimulation experiments with similar laser power and detector gain settings. The bleaching of YpH fluorophores then achieved by increasing the laser power by the factor of 2-3. We observed that there are mostly two types of decay in YpH fluorescence; (a) exponential in ~30% and (b) stepwise in ~70% out of total analysed events (*n* = 277). We selected these stepwise events for further analysis of Sb2 molecules.

We further analyzed exponential decays of the bleaching events of YSpH. The average time constant (τ) is ~30 s (*n* = 14) which describes that on average it takes 30 s to bleach 63% of the total number of Sb2 molecules present on a vesicle; i.e., three YSpH molecules bleach out of total five in 30 s. Therefore, it is likely (more than 10% probability) that two YSpH will bleach simultaneously, especially following the start of the bleaching

procedure. In agreement, the percentage of events with the double amplitude (Fig. 20Aii) of the total bleaching events was 16.6%).

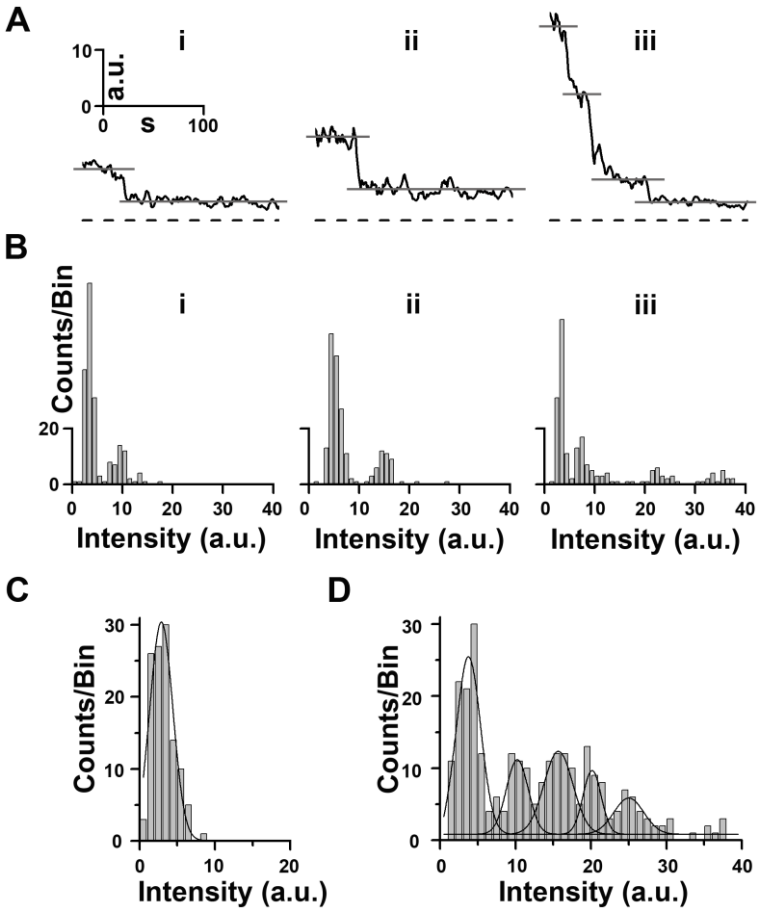

Figure 20: Photo bleaching of YSpH-labelled vesicles confirms the number of Sb2 molecules present on a single astrocytic vesicle. (**A**) Examples of time dependent changes in the fluorescence intensity of individual vesicles with abscissas showing the 'Intensity (a.u.)' and ordinates the 'Time (s)': (**Ai**) a small step decrease in YpH fluorescence, (**Aii**) step decrease by the factor of two compared to first event and (**Aiii**) an event with three step decrease in YpH fluorescence. In the panel (**A**), dashed line shows the baseline (zero-line) and the grey line denotes the fluorescence intensity level before discrete steps. (**B**) The respective amplitude distributions of the fluorescence intensity of each event shown in the panel (**A**). In the panel (**B**), 1st amplitude plot in each case denotes the lowest intensity observed. (**C**) Background, which was obtained by measuring the fluorescence intensity of the vesicle surroundings after 180 s of bleaching, recorded from 108 events (R^2 = 0.95; n = 108; bin width = 1.5 a.u.). (**D**) Combined plot of baseline and a decrease in the intensity after bleaching of YSpH-labelled vesicles, recorded from the same events (R^2 = 0.91; n = 277; bin width = 1.5 a.u.). The Gaussian curves are fitted using the Levenberg-Marquardt minimization fit keeping the standard deviation as determined in the background shown in (**C**) and using equation of form Counts/bin = $\{A/[\sigma(\sqrt{2\pi})]\}\times\exp\{-[(\text{Intensity}-\mu)^2/2\sigma^2]\}$. The values of A (area under curve) and μ (mean value of each peak) for these Gaussian fits are given in Tab. 6.

Fig. 20A displays three images of a vesicle recorded in an astrocyte that was exposed to NH_4Cl. (i) a small step decrease in YpH fluorescence, (ii) step decrease by the factor of two compared to first event and (iii) an event with three step decreases in YpH fluorescence. While analysing the responses from individual vesicles, we observed three patterns of YSpH fluorescence intensity changes (Fig. 20A). To estimate the mean value of these steps we plotted frequency distribution plots for individual events shown in Fig. 20A. We can clearly notice that these events show stepwise decay while bleaching of YSpH fluorescence (Fig. 20B). To determine the distribution of the background fluorescence (Fig. 20C) in the above experiments, we measured the fluorescence intensity near the vesicles, which are considered for further analysis (n = 108 events). This yielded a distribution with the mean value 2.89 ± 0.1 a.u (mean ± s.e.m.). The Gaussian curves of the form Counts/bin (a.u.) = $\{A/[\sigma(\sqrt{2\pi})]\} \times \exp\{-[(\text{Intensity (a.u.)} - \mu)^2/2\sigma^2]\}$ were fitted to the data. Values of the area under the curve (A), sigma (σ) and the mean peak (μ) for these Gaussian fits are given in Tab. 6.

Table 6: Photo bleaching experiment: Area under the curve (A) and mean value of each peak (μ) obtained from Gaussian curves.

Gaussian fits		A (mean ± s.e.m.)	Sigma (σ)	μ (mean ± s.e.m.)
Background		116 ± 6	1.51	2.89 ± 0.1
Steps	1st	99 ± 9	1.49	3.76 ± 0.1
	2nd	38 ± 10	1.33	10.22 ± 0.3
	3rd	55 ± 16	1.83	15.68 ± 0.4
	4th	26 ± 12	1.04	20.14 ± 0.4
	5th	25 ± 13	1.90	25.02 0.8

Fig. 20D shows a distribution of amplitudes of steps in the fluorescence after YSpH bleaching fluorescence (R^2 = 0.95; n = 108). We obtained σ from single Gaussian fit for background which equals 1.5 a.u. (see Tab. 6). Then we used this σ value to fit multiple Gaussians curves in the case of bleaching steps data. The respective values in the Tab. 6 give insight into the number of fluorescent entities present on a vesicle membrane. The first mode corresponds to the background and the second mode is designated for one YSpH molecule. Here, in photo bleaching experiments we confirm that the one unit mentioned in Fig. 18 is actually the one Sb2 molecule. If the modal peaks represent units or molecules, then these should represent simple integer multiples. This is confirmed in Fig. 20D where fluorescence intensity is distributed as multiples of a fundamental quantal unit. (R^2 = 0.91;

n = 277). Hence, these results indicate that there is a maximum of five molecules of YSpH in an astrocytic vesicle.

4.7 DETERMINATION OF ENDOGENOUS SB2 MOLECULES BASED ON QUANTIFICATION OF THE RATIO BETWEEN NUMBER OF EXOGENOUS AND ENDOGENOUS SB2 MOLECULES

To obtain the number of endogenous Sb2 molecules present on individual astrocytic vesicles, we used Sb2 immunolabelling of astrocytes transfected to express YSpH. Such individual astrocytes contain a mixture of vesicles, those laden with endogenous Sb2 alone (Atto positive, YpH negative) along with others that are dually-laden with both endogenous Sb2 and YSpH (Atto and YpH positive) (Fig. 21A left and 21B). Additionally, we compared the Sb2 immunoreactivity Atto signals of dually-laden vesicles to those of native vesicles from untransfected astrocytes.

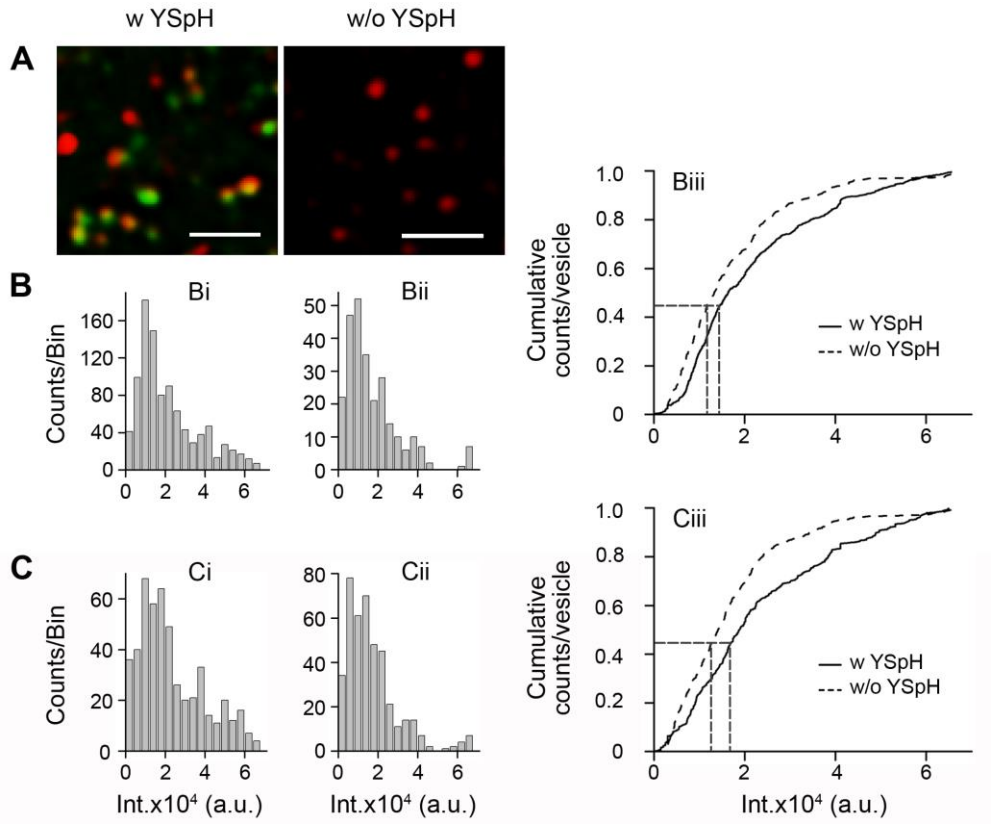

Figure 21. Quantification of the ratio between the number of YSpH and endogenous Sb2 molecules in astrocytic vesicles. (**A**) Left fluorescent micrograph shows vesicles in cells transfected by YSpH and labelled by the Atto red dye (note that not all vesicles are labelled by both fluorophores), whereas the right panel shows vesicles in astrocytes labelled by the Atto dye only. Scale bar: 10 μm. (**B-C**) We obtained the

distributions of (Atto) fluorescence intensity of Sb2 immunolabelled vesicles containing only endogenous Sb2 (w/o YSpH) and those that additionally contain exogenous Sb2 in form of YSpH (w YSpH). (**B**) Measurements were performed on vesicles within astrocytes expressing YSpH; some vesicles contained both endogenous Sb2 and YSpH (**Bi**) (n = 958), while other were devoid of YSpH expressing only endogenous Sb2 (**Bii**) (n = 262). (**Biii**) The normalized cumulative counts of the Atto intensity show significantly different distributions (Kolmogorov-Smirnov test, D = 0.134, $P < 0.001$). The vertical dotted lines drawn indicate the median value of 18772 a.u. (with YSpH) and 14115 a.u. (without YSpH) for Atto signals; horizontal dotted line indicates 50% of the total vesicle population. The difference between these two median values (4657 a.u.) likely denotes the quantum fluorescence of exogenous Sb2, i.e. YSpH, which was ~1/3 of that found in vesicles containing only endogenous Sb2. (**C**) Similar distribution as in (**B**), only that we measured Atto fluorescence intensities of Sb2 immunolabelled vesicles in YSpH transfected (**Ci**) (n = 499) and in non-transfected astrocytes (**Cii**) (n = 419), respectively. (**Ciii**) The normalized cumulative counts of the Atto intensity show significantly different distributions (Kolmogorov-Smirnov test, D = 0.184, $P < 0.001$); the median values at 16316 a.u. and 13382 a.u. for Atto signals of w and w/o YSpH vesicles and the difference between these two median values (2934 a.u.) suggests that exogenous Sb2 molecules represent ~1/5 of the number of endogenous Sb2 molecules; dotted lines as in (**B)**.

The distributions and cumulative plots of Atto fluorescence intensity of Sb2 immunolabelled vesicles that besides endogenous Sb2 (w/o YSpH; n = 262) contain exogenous Sb2 in form of YSpH (w YSpH; n = 958) show larger median values for Atto signals (Fig. 21B); the additional fluorescence of vesicles containing both endogenous and exogenous Sb2 was only ~0.33 of that found in vesicles containing only endogenous Sb2, indicating that for every one molecule/quantum of YSpH there are ~3 molecules of endogenous Sb2. A similar ratio was obtained when comparing Sb2 immunoreactivity/Atto signals from individual vesicles (n = 419) of untransfected astrocytes to those from dually-laden vesicles (n = 499) of YSpH transfected astrocytes (Fig. 21C); the additional Atto fluorescence of vesicles containing both endogenous and exogenous Sb2 was ~0.22 of that found in endogenous Sb2-only vesicles, which translates to ~5 endogenous Sb2 molecules for every YSpH molecule.

5 DISCUSSION

We have introduced a new approach to label secretory vesicles in astrocytes with newly designed recombinant Sb2 protein marked with different fluorescent tags and used super-resolution microscopy to visualize them in a living cell. We measured the diameter of different peptidergic and glutamatergic vesicle types in astrocytes. To determine the compartmentalization of proteins in vesicles of astrocytes (Mohrmann et al., 2010) we measured the length of Sb2 on a single vesicle in live cells *in vitro*. The length of Sb2 marked with YpH in vesicle lumen and with a fluorescent protein (mCherry) or a dye conjugated with antibodies against Sb2 (Atto) present on the cytoplasmic site was 57 and 65 nm, respectively. These measurements are in accordance with theoretical values of ~54 nm and 75-80 nm, respectively, given for the length of uncoiled Sb2, pHluorin, mCherry and antibodies (Ellena et al., 2009; Rizzo et al., 2009a; Sutton et al., 1998). As coiled Sb2 has three α-helices (I: 36-54 aa, II: 77-88 aa and III: 93-115 aa) (Ellena et al., 2009) and the distance between two adjacent aa residues in the helical form of peptide or protein is lesser by ~0.15 nm than in an elongated form (Lehninger, 1975; Stryer, 1995) coiled Sb2 (containing total of 51 coiled aa) should be about ~8 nm shorter compared to an uncoiled version. Consequently, the theoretical expectations for the above measurements then would be ~47 nm and ~67-72 nm, values that can be readily observed in YpH-mCherry (Fig. 14) and YpH-Atto (Fig. 13F) distributions around the peak measurements. Thus, it is likely that we have been observing a mixture of uncoiled and coiled Sb2; alternatively, the jitter in the measurement could be technical in nature (e.g., already mentioned variability in fluorophore alignments with respect to the imaging plane).

5.1 NONUNIFORM DISTRIBUTION OF SB2 ON THE VESICLE MEMBRANE

We measured the intensity of YpH and Atto from SIM images and classified YpH/Sb2 pairs into various categories based on the configurations or patterns of these fluorophores on astrocytic vesicles (Fig. 13). The most common observed pattern A likely represents a vesicle in which the number of Sb2 molecules is relatively low, perhaps only one molecule, because absolute intensities of YpH and Atto were comparable (Fig. 13A, middle). The pattern B whereby Atto fluorophore exhibited approximately three times higher fluorescence intensity than YpH intensity (Fig. 13B, middle) may be attributed to such individual puncta or vesicles where YSpH-positive Sb2 molecules, as well as endogenous Sb2, were decorated by Atto fluorophores. These images likely correspond to the clustering of Sb2, as noted previously by an *x*-ray study (Castorph et al., 2010). Previous reports indicate that Sb2 undergoes dimerization specifically at the transmembrane domain (Fleming and Engelman, 2001; Laage and Langosch, 1997). YpH and Atto pattern C (Fig. 13C, middle) offers a dichotomous interpretation: (i) either the

orientation of the Atto cluster is not parallel to the imaging plane or (ii) there may be two vesicles placed one over the other. The least common image observed pattern D (Fig. 13D, middle) was interpreted as Atto molecules present on two extremes of a vesicle circumference, while YpH is situated between two Atto puncta.

Although it is tempting to use the distance between two peaks of Atto signal enveloping or flanking the YSpH signal to coarsely estimate the vesicle diameter, such measurements could cause errors associated with size and positioning of antibodies and we have rather developed an alternative strategy to obtain the estimate of vesicular size in live astrocytes. there can also be an underestimation of the distance between fluorophores tagged on N- and C- termini of Sb2. Due to 2D-projection (if the molecules are not in the same plane), the orientation of Sb2 protein on the vesicle membrane will be different and to visualize this in the focal plane will be different as well. If the plane of protein is not parallel with the image or focal plane then, one can measure the projection of real protein and that's how we may underestimate the length of the protein.

5.2 VESICLE DIAMETER DETERMINED BY A LUMEN-FILLING APPROACH

Although several approaches have been used to measure vesicle diameter in astrocytes (Balaji and Ryan, 2007; Bowser and Khakh, 2007; Kreft et al., 2004), here we used a new approach based on Sb2 tagging in conjunction with the filling of vesicular lumen by an appropriate dye. After staining acidic organelles with LysoTracker dye, we obtained the apparent diameter of co-labelled YSpH vesicles as 305 ± 4 nm in live astrocytes. These data are in agreement with the measurements of vesicles tagged with Sb2 in live astrocytes investigated by evanescence wave microscopy; those vesicles had an apparent diameter ~312 nm (Malarkey and Parpura, 2011). In our measurements, only a subset of vesicles were interrogated due to the fact that a vesicle expressing a visible YSpH requires optimized pH in the vesicle lumen along with co-labelling with LysoTracker. Namely, LysoTracker stains mostly acidic compartments of astrocytes (Potokar et al., 2008), whereas YSpH becomes fluorescent once the fusion pore is open or by other mechanisms that lead to alkalization.

5.3 HOW MANY SB2 MOLECULES ARE PRESENT IN AN ASTROCYTIC VESICLE?

Some previous reports provide information about the number of Sb2 proteins/SNARE complex present on a vesicle membrane or number/ratio involved in fusion of a vesicle membrane with the plasma membrane in neurons (Burrone et al., 2006; Ellena et al., 2009;

Hua et al., 2011; Rizzo et al., 2009b; Sutton et al., 1998; Vardjan et al., 2007). Based on the changes in YSpH fluorescence and on the assumption that recombinant YSpH is loaded into vesicles in similar proportion as native Sb2, we estimated the number of Sb2 molecules present in an astrocytic vesicle, as well as the number of Sb2 molecules involved in fusion pore formation.

The fluorescence intensity patterns after application of ATP or NH_4Cl were different, indicating that addition of ATP makes visible only those YSpH molecules that are experiencing an alkaline milieu close to the fusion pore. This is an intriguing finding as it may point out to an unappreciated mechanism for pH buffering of vesicular lumen and it should be explored in the future. Alternatively, there could be a subpopulation of vesicles at the membrane that fuse when astrocytes are stimulated with ATP or vesicles are clustered and only some have access to the extracellular alkaline medium. On the other hand, the addition of NH_4Cl makes all the content of vesicle lumen alkaline because ammonia in solution diffuses across cell membranes and increases pH (Roos and Boron, 1981; Shroff et al., 2007). Therefore, in single-vesicle experiments, pH change by ATP elicits fluorescence of a limited portion of all available luminal vesicle pH-sensitive fluorescent proteins or a limited number of vesicles in a cluster. The amplitude distribution plot for ATP shows a single mode (Fig. 18Cii). The amplitude distribution plot for NH_4Cl with multiple modes (Fig. 18Ciii) signifies that after stimulation, all units of YSpH present in a vesicle lumen are fluorescent. The mean value obtained from each curve was equidistant (Fig. 18E), which indicates the apparent number of Sb2 molecules present in a single vesicle. The results show that there is at least one and not more than five Sb2 molecules present on an astrocytic vesicle. Most likely only one Sb2 molecule is involved in initial fusion pore formation during the merger between vesicle and plasma membranes in astrocytes.

The time-dependent intensity profile for each fluorescent punctum present in a cell after stimulation with ATP and NH_4Cl demonstrated three different types of events (Fig. 18B). The most abundant event in an astrocyte occurs after the addition of NH_4Cl. ATP influences two types of events: one shows a step increase in fluorescent intensity after ATP that is further enhanced by addition of NH_4Cl and another type of event also shows a step increase after ATP but, after approximately 1 min, it returns to the initial intensity, which then increases with addition of NH_4Cl. This rare event may be due to the fact that a secretory vesicle situated close to the plasma membrane can form a fusion pore that is stable (Rizzo et al., 2009a).

In a full fusion event there should not be any difference in fluorescence intensity compared to NH_4Cl. One of the possible explanations of the different fluorescence evoked by ATP and NH_4Cl applications is that different stimulations may affect different modes of

exocytosis. In addition to full fusion exocytosis also transient exocytosis was confirmed in astrocytes in several previous studies (e.g. Bowser and Khakh, 2007; Malarkey et al., 2011). In agreement with this notion we should mention that we used the relatively mild stimulation with 100 μM concentration of ATP, which may promote transient exocytosis. In the case of transient exocytosis, only some YSpH (perhaps those located close to the fusion pore) may increase its fluorescence, while in contrast the application of NH_4Cl would affect all YSpH molecules in a vesicle due to the strong alkalization of the vesicular lumen. This is an intriguing finding as it may point out to an unappreciated mechanism for pH buffering of vesicular lumen and it should be explored in the near future.

We also obtained comparable estimated number of Sb2 molecules using photo bleaching of alkalized YSpH-laden vesicles. Thus, the estimated numbers of Sb2 molecules per vesicle in live astrocytes (Figs. 18 and 20) appear similar using two approaches (ATP or NH_4Cl-mediated YSpH increase and photo bleaching of NH_4Cl-alkalized YSpH-laden vesicles) that cross-check each other. The distributions and cumulative plots of Atto fluorescence intensity of Sb2 immunolabelled vesicles that besides endogenous Sb2 contain exogenous Sb2 in form of YSpH indicating that for every one molecule/quantum of YSpH there are ~3-5 molecules of endogenous Sb2 molecules for every YSpH molecule. This finding further supports the idea that vesicles in astrocytes contain an order of magnitude smaller number of Sb2 molecules then reported previously for isolate neuronal or synaptic vesicles (Takamori et al., 2006).

6 CONCLUSION

We confirmed all of the hypotheses considered at the beginning of experiments. We described the architecture of a single astrocytic vesicle. The positioning and relative intensities of the two fluorophores enabled us to estimate, how Sb2 is packed in a single vesicle in astrocytes. The number of molecules was estimated by plotting the intensity distributions of each fluorophore and from photo bleaching of YSpH we were able to interpret the number of molecules per vesicle. The use of pH-sensitive fluorescent proteins revealed the details of fusion of the vesicle membrane with the plasma membrane. As the fusion pore opens the acidic pH of the vesicle lumen gets alkaline and the fluorescence of pH-sensitive proteins intensifies. Our study demonstrates the nano-architecture of Sb2 on a single vesicle in astrocytes. We estimated the diameter of different peptidergic and glutamatergic vesicle types by super-resolution microscopy. SIM with better spatial and axial resolution shows reduced percentage of colocalization between the two fluorescent tags compared to that from CLSM. The deep analysis of SIM images revealed that these two different tags (YpH and Atto) are mostly present at some distance as we observed the pairs which are maximum colocalized are ~15% of the total vesicles present in astrocytes as described in Fig. 13. We resolved the average distance between pHluorin protein present in vesicle lumen and another fluorescent tag situated on the surface of vesicle membrane as 65 ± 2 nm. This is in accordance with theoretical values given for total length of Sb2, pHluorin and antibodies (Ellena et al., 2009; Lehninger, 1975; Rizzo et al., 2009b; Stryer, 1995; Sutton et al., 1998).

We classified YpH-Atto (green-red) pairs and analysis describes that the arrangement of Atto with respect to YpH fluorophores are mostly present in four configurations. Out of these configurations, the most common arrangement has one molecule of each YpH and Atto across the vesicle membrane. The second common configuration has one or two molecules of YpH in the lumen and more than one molecule of Atto on surface of vesicle membrane. These Atto fluorophores are found in clusters on the vesicle membrane, which are also known as nano-aggregates of protein molecules. The presence of these clusters may be due to the polarization effect induced by attachment of YSpH through the vesicle membrane or may be due the presence of amino acid charges on protein itself. The data shows that these Sb2 proteins are mostly clustered or aggregated which is in accordance with previous literature that proteins form nano-aggregates. There are several approaches employed for the measurement of vesicle diameter. We obtained the apparent diameter of astrocytic vesicles as 305 ± 4 nm by staining the vesicle lumen with LysoTracker and then imaging the live astrocytes with SIM. As LysoTracker stains endosomes and lysosomes, we can say that these are mostly bigger in sizes compared to peptidergic and glutamatergic vesicles.

The single-vesicle experiments on live astrocytes with YSpH revealed important interpretations about nano-architecture of a single astrocytic vesicle. First interpretation is the intensity profile for each fluorescent puncta present in the cell after stimulation with ATP and NH_4Cl demonstrate three different types of evokes. Out of these evokes the first type shows evoke only after addition of NH_4Cl, second type includes evoke after ATP and the subsequent enhancement after NH_4Cl addition and the third type includes evoke after ATP but approximately after one minute it comes back to the baseline then, again the intensity shoots up by the addition of NH_4Cl. Second interpretation is the pH change elicits fluorescence of a limited portion of all available luminal vesicle pH-sensitive fluorescent proteins. This has been confirmed by plotting the histograms for baseline, after ATP and NH_4Cl stimulation. One may think that the process of alkalization of vesicle lumen is a very fast process and therefore, the intensity profiles should be same after ATP or NH_4Cl application but, with these stimulations the intensity patterns are different which suggest that may be addition of ATP make only those molecules alkaline which are present close to the vesicle membrane and has the contact with plasma membrane via narrow fusion pore which further leads to the fusion. These molecules may hinder the further alkalization of vesicle lumen but, addition of NH_4Cl made all the content of vesicle lumen to be alkaline because it can enter through the vesicle membrane in the form of ammonium ion whereas, ATP cannot pass through a vesicle membrane without a fusion pore as it has 30 times higher molecular weight than ammonium ion therefore, NH_4Cl is used as the saturated alkalization of the lumen (Sinha et al., 2011) it makes all the pHluorin molecules fluorescent which are present in the lumen.

We described several key characteristics of the astrocytic vesicle architecture at sub-vesicular resolution. These significant advancements of nano-architecture of a secretory vesicle will help to identify molecular characteristics of vesicle-associated SNARE proteins at nanometer resolution in living cells. Our findings will contribute to the progress in the field of cell biology especially for cell-to-cell communication. Answers to our hypotheses will provide significant advancements to identify molecular characteristics of vesicle-associated SNARE proteins at nanometre resolution in living cells. In summary, the results provide new insight into the nano-architecture of Sb2 on an astrocytic vesicle, which is playing a role in vesicle fusion and gliotransmitter release from astrocytes. These results will contribute to progress in the field of cell biology of cell-to-cell communication. Our measurements revealed that in astrocytes the total number of exogeneous Sb2 molecules is less than five per vesicle and that only one Sb2 molecule is involved in the initial fusion pore formation during the merger of a vesicle membrane with the plasma membrane.

7 SUMMARY (POVZETEK)

7.1 SUMMARY

The exocytic transmitter release is regulated by the SNARE complex, which contains a vesicular membrane protein, synaptobrevin2 (Sb2). However, the arrangement of Sb2 molecules on vesicles is unclear. Using super-resolution fluorescence microscopy, we studied the prevalence and distribution of endogenous and exogenous Sb2 in single vesicles of astrocytes, the most abundant glial cells in the brain. The study of single vesicle architecture in astrocytes is important to elucidate the mechanism of exocytosis, which is one of the key processes of gliotransmitter release in astrocytes. To resolve the architecture of a single vesicle in astrocytes we determined: (i) diameters of vesicles carrying Sb2, (ii) the size and (ii) arrangement of vesicular Sb2 molecules, as well as (iii) the average number of Sb2 molecules per vesicle in live astrocytes. Secretory vesicles in astrocytes transport three classes of gliotransmitters: (i) amino acids; glutamate and D-serine (ii) nucleotides; adenosine 5'-triphosphate (ATP) and (iii) peptides; atrial natriuretic peptide (ANP) and brain-derived neurotrophic factor (BDNF). We labelled different types of vesicles by selecting antibodies against specific moieties.

The exact number of Sb2 molecules or SNARE complexes present on the vesicle membrane or involved in the fusion of a vesicle membrane with the plasma membrane is still questioned. In one of the studies on neurons, it was proposed that there are seventy Sb2 molecules present on a synaptic vesicle. On the other hand, other groups have shown that only a few Sb2 molecules are required for the fusion of synaptic vesicle with the plasma membrane. There is no previous direct study which signifies the arrangement of Sb2 on a synaptic vesicle. To this end, the number of Sb2 on the astrocytic vesicles remains unknown.

To assess the number and the arrangement of Sb2 on the vesicle membrane we used fluorescent proteins and structured illumination microscopy (SIM) as super-resolution fluorescence microscopy. With SIM we estimated the length between two fluorophores attached to the N- and C- termini of Sb2. In addition, these measurements showed that, even though the resolution of SIM is ~100 nm, we can accurately measure dimensions below this limit.

The experiments were performed by utilizing newly developed yellow shifted pHluorin protein (YSpH). First, we expressed YSpH in astrocytes and immunolabelled them with anti-Sb2 antibody in combination with Atto dye, to measure the distance between the two fluorophores (YpH and Atto). YpH is attached genetically to the C-terminus of Sb2, which is present in the vesicle lumen, while 1–18 amino acids of N-terminus at the cytoplasmic

site was recognized by either fluorescently labelled antibodies or we used recombinant fusion protein between N-terminus of Sb2 and mCherry. The two termini of Sb2 were labelled with markers that can be excited by different wavelengths and thus could be spectrally resolved. To validate our approach, we have also performed another set of experiments, where we used two other constructs, namely mCherry-YSpH (the two fluorophores are adjacent to each other) and YSpH-7aa-mCherry (the two fluorophores are separated with seven amino acids). In the latter two constructs, the two fluorophores were already part of the Sb2; therefore we avoided further immunolabelling of Sb2 fragment.

The length of Sb2 marked with YpH in vesicle lumen and with a fluorescent protein (mCherry) or a dye conjugated with antibodies against Sb2 (Atto) present on the cytoplasmic site was 57 and 65 nm, respectively. These measurements are in accordance with theoretical values of ~54 nm and 75-80 nm, respectively, given for the length of uncoiled Sb2, and by taking into account the size of pHluorin, mCherry and antibodies. However, coiled Sb2 has three α-helices and the distance between two adjacent amino acid residues in the helical form of peptide or protein is lesser by ~0.15 nm, than in an elongated form. Coiled Sb2 (containing total of 51 coiled amino acids) should therefore be about ~8 nm shorter compared to an uncoiled version. Consequently, the theoretical expectations for the above measurements then would be ~47 nm and ~67-72 nm. The data obtained in our study have shown similar values, which were determined as peak-to-peak distances of mCherry-YpH and YpH-Atto fluorescence intensity profiles. Thus, it is likely that we have been observing a mixture of uncoiled and coiled Sb2; alternatively, the jitter in the measurement could be due to the random error of respective measurements.

The intensity measurements of YpH and Atto from SIM images classified YpH/Atto pairs into various categories, based on the configurations or patterns of these fluorophores on astrocytic vesicles. The most commonly observed pattern likely represents a vesicle in which the number of Sb2 molecules is relatively low, perhaps only one molecule, because absolute intensities of YpH and Atto were comparable. The pattern whereby Atto fluorophore exhibited approximately three times higher fluorescence intensity than YpH intensity may be attributed to such individual puncta or vesicles where YSpH-positive Sb2 molecules, as well as endogenous Sb2, were decorated by Atto fluorophores. These images likely correspond to clustering of Sb2, as noted previously by an x-ray study. Previous reports indicate that Sb2 undergoes dimerization specifically at the transmembrane domain. YpH and Atto pattern offers a dichotomous interpretation: (i) either the orientation of the Atto cluster is not parallel to the imaging plane or (ii) there may be two vesicles placed one over the other. The least common image observed pattern was interpreted as Atto molecules present on two extremes of a vesicle circumference, while YpH is situated between two Atto puncta. There can also be an underestimation of the distance between fluorophores tagged on N- and C- termini of Sb2. Due to 2D-projection (if the molecules

are not in the same plane), the orientation of Sb2 protein on the vesicle membrane will differ and to visualize this in the focal plane will again distort the result.

Although it is tempting to use the distance between two peaks of Atto signal enveloping or flanking the YSpH signal to coarsely estimate the vesicle diameter, such measurements could cause errors associated with the positioning of antibodies. Thus we rather measured vesicular diameters by an alternative approach in live astrocytes. Although several approaches have been used previously to measure vesicle diameter in astrocytes, we used a new approach based on Sb2 tagging and filling the lumen of vesicles with LysoTracker. As LysoTracker stains all acidic compartments, we can separate larger structures, which likely represent endosomes and lysosomes from smaller peptidergic and glutamatergic vesicles. Imaging was performed with SIM. The apparent diameter of selected YSpH-laden vesicles was 305 ± 4 nm in live astrocytes, in good agreement with measurements of vesicles tagged with Sb2 in live astrocytes and investigated using evanescence wave microscopy (where a diameter of ~312 nm was obtained). In our measurements, only a subset of acidic vesicles were interrogated, which were expressing also YSpH, while YSpH requires optimized pH. Namely, LysoTracker stains mostly acidic compartments of astrocytes, whereas YSpH becomes fluorescent once the fusion pore is open or by other mechanisms that lead to alkalization.

As pHluorin is non-fluorescent at acidic pH, we stimulated astrocytes with ATP and NH_4Cl solutions to increase the pH. The fluorescence intensity analysis in this experiment was used to determine the number of Sb2 molecules present on a single vesicle in astrocytes. To affirm that the fluorescence intensity correlates with the total number of Sb2 molecules per vesicle, we then performed photo bleaching of fluorophores. In addition, to assess the number of Sb2 molecules necessary for the formation of fusion pores, we treated cells with ATP to stimulate Ca^{2+}-dependent exocytosis and determined the fluorescence intensity.

The time-dependent intensity profile for each fluorescent punctum present in a cell after stimulation with ATP and NH_4Cl demonstrated three different types of events. The most abundant event in an astrocyte occurs after the addition of NH_4Cl. ATP influences two types of events: one shows a step increase in fluorescent intensity after ATP that is further enhanced by the addition of NH_4Cl and the other type of event shows a step increase after ATP but, approximately after one minute, it returns to the initial intensity, which then increases with the addition of NH_4Cl. This rare event may be due to the vesicular formation of a stable fusion pore. In a full fusion event there should not be any difference in fluorescence intensity compared to NH_4Cl. In addition to full fusion exocytosis also transient exocytosis was confirmed in astrocytes in several previous studies. In agreement

with this, the mild stimulation with 100 μM concentration of ATP likely promoted transient exocytosis.

One may think that the process of alkalization of vesicle lumen is a very fast process and therefore, the intensity profiles should be same after ATP or NH_4Cl application but, with these stimulations the intensity patterns are different. Therefore, the addition of ATP likely affects only Sb2 molecules which are located in the close vicinity of the open fusion pore. The addition of NH_4Cl, on the other hand alkalizes all the vesicle lumen by passing ammonia through the vesicle membrane (vesicle membrane is not permeable for ATP which has ~30 times higher molecular weight).

Alternatively, there could be a sub-population of vesicles at the membrane that fuse when astrocytes are stimulated with ATP or vesicles are clustered and only some have access to the extracellular alkaline medium. The amplitude distribution plot for ATP shows a single mode, while the amplitude distribution plot for NH_4Cl with multiple modes signifies that after stimulation, all units of YSpH present in a vesicle lumen are fluorescent. The mean value between consequent peaks in the multimodal curve was equidistant, which indicates that each peak represents one Sb2 molecule present in a single vesicle.

The results show that there is at least one and not more than five Sb2 molecules present on an astrocytic vesicle. Most likely only one Sb2 molecule is involved in the initial fusion pore formation during the merger between vesicle and plasma membranes in astrocytes. The estimated number of Sb2 molecules obtained by photo bleaching of alkalized YSpH-laden vesicles is comparable to the ATP or NH_4Cl-mediated YSpH increase. This finding further supports the idea that vesicles in astrocytes contain an order of magnitude smaller number of Sb2 molecules than reported previously for isolate neuronal or synaptic vesicles.

We confirmed all of the hypotheses considered. We described the architecture of a single astrocytic vesicle. The positioning and relative intensities of the two fluorophores were used to determine, how Sb2 is packed in a single vesicle in astrocytes. Super-resolution optical microscopy was used to measure the exact length between two fluorophores. We propose that the exact number of exogenous Sb2 molecules present on the vesicle membrane in astrocytes is no more than five, while one is sufficient for the initial fusion pore formation during the merger of a vesicle with the plasma membrane. Our findings will contribute to the progress in the field of cell biology especially regarding the cell-to-cell communication. Answers to our hypotheses will provide significant advancements to identify molecular characteristics of vesicle-associated SNARE proteins at nanometre resolution in living cells.

7.2 POVZETEK

Sproščanje signalnih molekul z eksocitozo uravnava skupina beljakovin, ki tvori kompleks SNARE. Kompleks SNARE med drugim vsebuje beljakovino sinaptobrevin2 (Sb2), ki je na mešičkih, njena razporeditev na mešičkih pa ni poznana. Z visokoločljivostno mikroskopijo smo raziskovali pojavnost in porazdelitev endogene in eksogene beljakovine Sb2 na posameznih mešičkih v astrocitih, najštevilčnejših celicah glije v možganih. Raziskave razporeditve molekul na posameznih mešičkih v astrocitih so pomembne za razumevanje mehanizmov eksocitoze, ki je eden ključnih procesov za sproščanje gliotransmiterjev iz astrocitov. Namen naše raziskave razporeditve molekul na posameznih mešičkih v astrocitih je bil oceniti več parametrov, in sicer premer mešičkov in povprečno število beljakovin Sb2 na površini mešičkov v astrocitih. Beljakovina Sb2, pomemben del kompleksa SNARE, je v astrocitih na sekrecijskih mešičkih, ki vsebujejo tri različne vrste gliotransmiterjev: (i) amino kisline; glutamat in D-serin (ii) nukleotide; adenozin 5'-trifosfat (ATP) in (iii) peptide; atrijski natriuretični peptid (ANP) in možganski nevrotropni dejavnik (angl. brain-derived neurotrophic factor; BDNF). Različne vrste mešičkov smo označili s protitelesi proti vsebini mešičkov, in sicer s protitelesi anti-ANP, anti-BDNF, anti-D-serine and anti-VGLUT1.

Natančno število molekul Sb2 ali število kompleksov SNARE na membrani mešička ali v procesu fuzije membrane mešička s plazmalemo še vedno ni poznano. Na osnovi ene izmed študij na nevronih, so raziskovalci ocenili, da je na sinaptičnem mešičku prisotnih sedemdeset molekul Sb2. Nekatere druge raziskovalne skupine pa so pokazale, da je za fuzijo sinaptičnega mešička s plazmalemo potrebno znatno manj molekul Sb2. Nobena študija do zdaj ni neposredno obravnavala razporeditve molekul Sb2 na mešičkih. Število molekul Sb2 na mešičkih v astrocitih ni poznano.

Pri študijah razumevanja mehanizma fuzije membrane mešička in plazmaleme je ključnega pomena poznavanje velikosti mešičkov in razporeditve molekul Sb2 na teh mešičkih. Da bi ugotovili število in razporeditev molekul Sb2 na membrani mešička, smo uporabili selektivne fluorescenčne beljakovine in visokoločljivostno mikroskopijo SIM (angl. structured illumination super-resolution fluorescence microscopy; SIM). S tehniko SIM smo ocenili razdaljo med dvema fluoroforjema pripetima na N- in C-konec molekule Sb2. Hkrati smo pokazali, da je kljub omejitvam ločljivosti pri SIM, ki je ~100 nm, mogoče natančno izmeriti dimenzije pod to mejo ločljivosti.

Poskusi so bili narejeni na novi različici rekombinantne beljakovine Sb2 s pripeto rumeno fluorescenčno beljakovino, občutljivo na pH (YSpH). Najprej smo v celice vnesli YSpH in jih nato označili s protitelesi proti Sb2 v kombinaciji z barvilom Atto in izmerili razdaljo med obema fluoroforjema (YpH in Atto). YpH je pripet na C-konec molekule Sb2, ki je v mešičku, 18 aminokislin dolgo zaporedje na N-koncu Sb2 pa je na citoplazemski strani in smo ga fluorescenčno označili s protitelesi ali pa smo uporabili konstrukt DNA, kjer je na

N-konec Sb2 pripet fluorofor mCherry. Oba konca molekule Sb2 sta bila tako označena z markerji, ki imajo različne valovne dolžine vzbujene in oddane svetlobe in jih je tako mogoče spektralno ločiti. Da bi tak pristop validirali, smo naredili še dodaten niz poskusov, kjer smo uporabili še dva konstrukta DNA, mCherry-YSpH (fluoroforja sta v tem primeru neposredno en zraven drugega) in YSpH-7aa-mCherry (fluoroforja sta ločena s sedmimi aminokislinami). Pri teh dveh konstruktih sta fluoroforja že del molekule Sb2, s čimer smo se izognili dodatnemu označevanju s protitelesi.

Izmerjena dolžina molekule Sb2, označena z YpH v lumnu mešička in z mCherry ali z barvilom Atto na citoplazemski strani mešička, je bila 57 nm (mCherry) in 65 nm (Atto). Te meritve se ujemajo s teoretičnimi vrednostmi ~54 nm in 75-80 nm, glede na dolžino nezvite molekule Sb2 ter z upoštevanjem velikosti pHluorina, mCherry in protiteles. Zvita molekula Sb2 ima tri α-vijačnice in razdalja med dvema sosednjima aminokislinama v vijačnici je za ~0.15 nm manjša kot pri nezviti obliki. Zvita molekula Sb2 (ki jo sestavlja 51 aminokislin) je zato od nezvite molekule Sb2 krajša za ~8 nm. Ob upoštevanju te vrednosti, bi morale biti teoretične vrednosti zgornjih meritev ~46 nm in ~67-72 nm. Srednje vrednosti dolžin molekule Sb2, ki smo jih izmerili, so primerljive s teoretičnimi vrednostmi. Razpršenost izmerjenih vrednosti bi lahko bila posledica meritev mešanice zvitih in nezvitih molekul Sb2, ali pa gre samo za naključno napako meritev.

Glede na razporeditev in intenziteto signalov fluoroforjev YpH in Atto na mešičkih astrocitov, smo meritve razdelili v več skupin. Najbolj pogosto smo opazili vzorec, kjer je število molekul Sb2 relativno nizko, morda je molekula Sb2 celo ena sama. Značilno za ta vzorec je bila primerljiva intenziteta signalov YpH in Atto. Opazili smo tudi vzorec, kjer je bila intenziteta signala Atto približno trikrat višja kot intenziteta signala YpH, signala pa sta bila prekrita. V tem primeru smo verjetno opazovali mešičke, v katerih so se protitelesa Atto vezala na endogene molekule Sb2 in na vnesene molekule Sb2 s pripeto YSpH. Poleg tega ta vzorec verjetno odraža skupek molekul Sb2. Prejšnje študije so pokazale, da so za polimerizacijo molekul Sb2 odgovorni transmembranski odseki teh molekul. Prekritost signalov YpH in Atto je verjetno posledica: (i) orientacije obeh fluoroforjev, ki sta sicer locirana na istem mešičku, je v prostoru poravnana s smerjo detekcije, ali (ii) opazujemo dva fluoroforja na različnih mešičkih, ki sta locirana eden nad drugim. Najredkeje smo opazili vzorec, kjer sta signala Atto prisotna na različnih polih mešička, med njima pa signal YpH. Razdaljo med dvema fluoroforjema smo najverjetneje podcenili, ker je mikroskopska slika dvodimenzionalna, snemamo pa tridimenzionalne strukture (kar pomeni, da posnamemo projekcijo opazovanih objektov na ravnino).

Čeprav bi lahko razdaljo med signaloma Atto uporabili za izračun premera mešička, bi bila taka meritev podvržena napakam zaradi lokacije fluoroforjev Atto, ki so verjetno redko postavljeni popolnoma na nasprotne strani (pola) mešička. Zato smo izmerili premer mešičkov v živih astrocitih tako, da smo v mešičke vnesli plazmide, ki kodirajo rekombinantne beljakovine Sb2 z YSpH in jih označili z barvilom LysoTracker, ki označi

lumen mešičkov. LysoTracker označi vse kisle celične organele, zato lahko z dvojnim označevanjem ločimo večje endosome in lizosome od manjših peptidnih in glutamatnih mešičkov. Tudi te poskuse smo opravili na mikroskopu SIM. Povprečni premer označenih mešičkov v astrocitih je bil 305 ± 4 nm. Ta vrednost je primerljiva z objavljenimi meritvami premerov mešičkov, ki vsebujejo Sb2, in so bile opravljene z metodo fluorescenčne mikroskopije s popolnim odbojem (kjer so izmerili povprečni premer ~312 nm). V naših poskusih smo analizirali premere manjšega deleža vseh mešičkov, ker LysoTracker označi kisle celične organele, YSpH pa najmočneje fluorescira v bazičnih pogojih (npr. ko se odpre fuzijska pora, kar privede do uhajanja protonov iz lumna mešička). Zaradi optimalne fluorescence YSpH, smo mešičke stimulirali z NH_4Cl, ki poviša pH znotrajceličnih organelov. V teh poskusih smo določili intenziteto fluorescence diskretnih točk, ki je sorazmerna s številom molekul Sb2 na posameznih mešičkih. Da intenziteta posameznih točk res ustreza številu molekul na posameznem mešičku, smo nato izvedli še poskus z bledenjem fluorescence. Fluorescenca posameznih molekul namreč zbledi v diskretnih skokih, katerih število ustreza številu molekul Sb2. Določili smo tudi število molekul Sb2, ki je potrebno za odprtje fuzijske pore, in sicer tako, da smo celice stimulirali z ATP in ponovno določili intenziteto fluorescence.

Časovni profil intenzitete fluorescence posameznih točk po stimulaciji z ATP in NH_4Cl smo razdelili v tri razrede. Najpogosteje smo opazili znaten porast intenzitete fluorescence po dodatku NH_4Cl. ATP pa je povzročil trajen ali, redkeje, prehoden porast intenzitete fluorescence. Prehodni porast intenzitete fluorescence verjetno odraža odprtje stabilne fuzijske pore, saj intenziteta ni dosegla ravni primerljive z NH_4Cl, kar bi se pri dogodku popolne fuzije zgodilo. Popolna in prehodna fuzija v astrocitih sta bili potrjeni že v številnih študijah. Naši rezultati kažejo, da relativno blaga stimulacija s 100 μM ATP preferenčno sproži prehodno fuzijo.

Alkalizacija mešičkov ni hiter proces, kar potrjujeta različna profila intenzitete fluorescence po stimulaciji z ATP in NH_4Cl. Omenjena razlika najverjetneje pomeni, da dodatek ATP vpliva najprej na molekule Sb2, ki so locirane blizu odprte fuzijske pore. NH_4Cl pa povzroči alkalinizacijo celotnega mešička znatno hitreje zaradi prehoda shozi celotno membrano (Membrane pa niso prehodne za ATP, ki ima ~30 krat večjo molsko maso). Morda pa obstaja populacija mešičkov, ki se odziva na stimulacijo z ATP, in v kateri je samo manjši del mešičkov lociran ob plazmalemi. Da različni stimulaciji vplivata na različno število molekul Sb2, smo potrdili tudi z analizo intenzitet fluorescence po posameznih stimulacijah. Porazdelitev amplitud intenzitete fluorescence po stimulaciji z ATP je bila normalna, medtem ko je imela porazdelitev po stimulaciji z NH_4Cl več vrhov. Oddaljenost med posameznimi vrhovi je bila enaka, zato lahko zaključimo, da je vsak vrh predstavljal eno molekulo Sb2 v posameznem mešičku. Število vrhov (molekul Sb2) v posameznem mešičku je bilo med ena in pet. En sam vrh po stimulaciji z ATP pa verjetno pomeni, da je za fuzijo mešička s plazmalemo dovolj ena sama molekula Sb2. Do istega zaključka smo prišli tudi s poskusi z bledenjem, kjer je bilo število molekul Sb2 v

posameznih mešičkih (skok navzdol v fluorescenci je najverjetneje odražal eno molekulo Sb2) primerljivo. Zaključimo lahko, da je število molekul Sb2 v mešičkih astrocitov za velikostni razred manjše od števila v mešičkih živčnih celic.

Potrdili smo vse zastavljene hipoteze. Opisali smo arhitekturo posameznih mešičkov v astrocitih, to je, velikost mešičkov, porazdelitev molekul Sb2 na njih in velikost teh molekul na membrani mešičkov. Določili smo tudi število molekul Sb2 v posameznih mešičkih (od ena do pet) in število teh molekul (ena sama), ki verjetno sodeluje pri fuziji mešičkov s plazmalemo. Te ugotovitve bodo pomembno prispevale k razumevanju procesov medcelične komunikacije in poglobile znanje na področju celične biologije. Korak naprej predstavlja zlasti napredek v razumevanju molekulskih značilnosti beljakovin SNARE, izmerjene v živih astrocitih.

8 REFERENCES

Abbe, E., 1873. Beiträgezurtheorie des mikroskops und der mikroskopischenwahrnehmung. Archiv für mikroskopische Anatomie, 9**:** 413-418

Bal-Price, A., Moneer, Z., Brown, G.C., 2002. Nitric oxide induces rapid, calcium-dependent release of vesicular glutamate and ATP from cultured rat astrocytes. Glia, 40**:** 312-323

Balaji, J., Ryan, T.A., 2007. Single-vesicle imaging reveals that synaptic vesicle exocytosis and endocytosis are coupled by a single stochastic mode. Proceedings of the National Academy of Science U S A, 104**:** 20576-20581

Bennett, J.P., Lowrie, M.B., 1992. Are neurotransmitter carriers cell-specific markers? Trends in Neurosciences, 15**:** 483-484

Bergami, M., Santi, S., Formaggio, E., Cagnoli, C., Verderio, C., Blum, R., Berninger, B., Matteoli, M., Canossa, M., 2008. Uptake and recycling of pro-BDNF for transmitter-induced secretion by cortical astrocytes. Journal of Cell Biology, 183**:** 213-221

Bergersen, L.H., Morland, C., Ormel, L., Rinholm, J.E., Larsson, M., Wold, J.F., Roe, A.T., Stranna, A., Santello, M., Bouvier, D., Ottersen, O.P., Volterra, A., Gundersen, V., 2012. Immunogold detection of L-glutamate and D-serine in small synaptic-like microvesicles in adult hippocampal astrocytes. Cerebral Cortex, 22**:** 1690-1697

Bezzi, P., Gundersen, V., Galbete, J.L., Seifert, G., Steinhauser, C., Pilati, E., Volterra, A., 2004. Astrocytes contain a vesicular compartment that is competent for regulated exocytosis of glutamate. Nature Neuroscience, 7**:** 613-620

Blasi, J., Binz, T., Yamasaki, S., Link, E., Niemann, H., Jahn, R., 1994. Inhibition of neurotransmitter release by clostridial neurotoxins correlates with specific proteolysis of synaptosomal proteins. Journal of Physiology Paris, 88**:** 235-241

Bowser, D.N., Khakh, B.S., 2007. Two forms of single-vesicle astrocyte exocytosis imaged with total internal reflection fluorescence microscopy. Proceedings of the National Academy of Sciences U S A, 104**:** 4212-4217

Brewer, J.M., Pollock, K.G., Tetley, L., Russell, D.G., 2004. Vesicle size influences the trafficking, processing, and presentation of antigens in lipid vesicles. Journal of Immunology, 173**:** 6143-6150

Budzinski, KristiÂ L., Zeigler, M., Fujimoto, BryantÂ S., Bajjalieh, SandraÂ M., Chiu, DanielÂ T., 2011. Measurements of the Acidification Kinetics of Single SynaptopHluorin Vesicles. Biophysical Journal, 101**:** 1580-1589

Burrone, J., Li, Z., Murthy, V.N., 2006. Studying vesicle cycling in presynaptic terminals using the genetically encoded probe synaptopHluorin. Nature Protocols, 1**:** 2970-2978

Cans, A.S., Hook, F., Shupliakov, O., Ewing, A.G., Eriksson, P.S., Brodin, L., Orwar, O., 2001. Measurement of the dynamics of exocytosis and vesicle retrieval at cell populations using a quartz crystal microbalance. Analytical Chemistry, 73**:** 5805-5811

Castorph, S., Riedel, D., Arleth, L., Sztucki, M., Jahn, R., Holt, M., Salditt, T., 2010. Structure parameters of synaptic vesicles quantified by small-angle x-ray scattering. Biophysical Journal, 98**:** 1200-1208

Ceccarelli, B., Hurlbut, W.P., Mauro, A., 1973. Turnover of transmitter and synaptic vesicles at the frog neuromuscular junction. Journal of Cell Biology, 57**:** 499-524

Coleman, C.G., Anrather, J., Iadecola, C., Pickel, V.M., 2009. Angiotensin II type 2 receptors have a major somatodendritic distribution in vasopressin-containing neurons in the mouse hypothalamic paraventricular nucleus. Neuroscience, 163**:** 129-142

Crippa, D., Schenk, U., Francolini, M., Rosa, P., Verderio, C., Zonta, M., Pozzan, T., Matteoli, M., Carmignoto, G., 2006. Synaptobrevin2-expressing vesicles in rat astrocytes: insights into molecular characterization, dynamics and exocytosis. Journal of Physiology, 570**:** 567-582

Dennison, M.E., 1971. Electron stereoscopy as a means of classifying synaptic vesicles. Journal of Cell Science, 8**:** 525-539

Di Maio, A., Skuba, A., Himes, B.T., Bhagat, S.L., Hyun, J.K., Tessler, A., Bishop, D., Son, Y.J., 2011. In vivo imaging of dorsal root regeneration: rapid immobilization and presynaptic differentiation at the CNS/PNS border. Journal of Neuroscience, 31**:** 4569-4582

Domanska, M.K., Kiessling, V., Stein, A., Fasshauer, D., Tamm, L.K., 2009. Single vesicle millisecond fusion kinetics reveals number of SNARE complexes optimal for fast SNARE-mediated membrane fusion. Journal of Biological Chemistry, 284**:** 32158-32166

Duan, S., Anderson, C.M., Keung, E.C., Chen, Y., Swanson, R.A., 2003. P2X7 receptor-mediated release of excitatory amino acids from astrocytes. Journal of Neuroscience, 23**:** 1320-1328

Ellena, J.F., Liang, B., Wiktor, M., Stein, A., Cafiso, D.S., Jahn, R., Tamm, L.K., 2009. Dynamic structure of lipid-bound synaptobrevin suggests a nucleation-propagation mechanism for trans-SNARE complex formation. Proceedings of the National Academy Sciences U S A, 106**:** 20306-20311

Fernandez-Suarez, M., Ting, A.Y., 2008. Fluorescent probes for super-resolution imaging in living cells. Nature Reviews Molecular Cell Biology, 9**:** 929-943

Fleming, K.G., Engelman, D.M., 2001. Computation and mutagenesis suggest a right-handed structure for the synaptobrevin transmembrane dimer. Proteins, 45**:** 313-317

Fusco, F.R., Martorana, A., Giampa, C., De March, Z., Farini, D., D'Angelo, V., Sancesario, G., Bernardi, G., 2004. Immunolocalization of CB1 receptor in rat striatal neurons: a confocal microscopy study. Synapse, 53**:** 159-167

Gandhi, S.P., Stevens, C.F., 2003. Three modes of synaptic vesicular recycling revealed by single-vesicle imaging. Nature, 423**:** 607-613

Gucek, A., Vardjan, N., Zorec, R., 2012. Exocytosis in astrocytes: transmitter release and membrane signal regulation. Neurochemical Research, 37**:** 2351-2363

Gustafsson, M.G., 2000. Surpassing the lateral resolution limit by a factor of two using structured illumination microscopy. Journal of Microscopy, 198**:** 82-87

Gustafsson, M.G., Shao, L., Carlton, P.M., Wang, C.J., Golubovskaya, I.N., Cande, W.Z., Agard, D.A., Sedat, J.W., 2008. Three-dimensional resolution doubling in wide-field fluorescence microscopy by structured illumination. Biophysical Journal, 94**:** 4957-4970

Halassa, M.M., Fellin, T., Haydon, P.G., 2007. The tripartite synapse: roles for gliotransmission in health and disease. Trends in Molecular Medicine, 13**:** 54-63

Han, K.S., Woo, J., Park, H., Yoon, B.J., Choi, S., Lee, C.J., 2013. Channel-mediated astrocytic glutamate release via Bestrophin-1 targets synaptic NMDARs. Molecular Brain, 6**:** 1-9

Hertz, L., Dringen, R., Schousboe, A., Robinson, S.R., 1999. Astrocytes: glutamate producers for neurons. Journal of Neuroscience Research, 57**:** 417-428

Hess, S.T., Girirajan, T.P., Mason, M.D., 2006. Ultra-high resolution imaging by fluorescence photoactivation localization microscopy. Biophysical Journal, 91**:** 4258-4272

Heuser, J.E., Reese, T.S., 1973. Evidence for recycling of synaptic vesicle membrane during transmitter release at the frog neuromuscular junction. Journal of Cell Biology, 57**:** 315-344

Hu, Y., Qu, L., Schikorski, T., 2008. Mean synaptic vesicle size varies among individual excitatory hippocampal synapses. Synapse, 62**:** 953-957

Hua, Y., Sinha, R., Thiel, C.S., Schmidt, R., Huve, J., Martens, H., Hell, S.W., Egner, A., Klingauf, J., 2011. A readily retrievable pool of synaptic vesicles. Nature Neuroscience, 14**:** 833-839

Huang, B., Bates, M., Zhuang, X., 2009. Super-resolution fluorescence microscopy. Annual Review of Biochemistry, 78**:** 993-1016

Jaim-Etcheverry, G., Zieher, L.M., 1969. Selective demonstration of a type of synaptic vesicle by phosphotungstic acid staining. Journal of Cell Biology, 42**:** 855-860

Jordan, R., Lemke, E.A., Klingauf, J., 2005. Visualization of synaptic vesicle movement in intact synaptic boutons using fluorescence fluctuation spectroscopy. Biophysical Journal, 89**:** 2091-2102

Jorgacevski, J., Potokar, M., Grilc, S., Kreft, M., Liu, W., Barclay, J.W., Buckers, J., Medda, R., Hell, S.W., Parpura, V., Burgoyne, R.D., Zorec, R., 2011. Munc18-1 tuning of vesicle merger and fusion pore properties. Journal of Neuroscience, 31**:** 9055-9066

Kacem, K., Lacombe, P., Seylaz, J., Bonvento, G., 1998. Structural organization of the perivascular astrocyte endfeet and their relationship with the endothelial glucose transporter: a confocal microscopy study. Glia, 23**:** 1-10

Karatekin, E., Di Giovanni, J., Iborra, C., Coleman, J., O'Shaughnessy, B., Seagar, M., Rothman, J.E., 2010. A fast, single-vesicle fusion assay mimics physiological SNARE requirements. Proceedings of the National Academy of Sciences U S A, 107**:** 3517-3521

Kim, S., Atwood, H.L., Cooper, R.L., 2000. Assessing accurate sizes of synaptic vesicles in nerve terminals. Brain Research, 877**:** 209-217

Kimelberg, H.K., Goderie, S.K., Higman, S., Pang, S., Waniewski, R.A., 1990. Swelling-induced release of glutamate, aspartate, and taurine from astrocyte cultures. Journal of Neuroscience, 10**:** 1583-1591

Kreft, M., Milisav, I., Potokar, M., Zorec, R., 2004. Automated high through-put colocalization analysis of multichannel confocal images. Computer Methods and Programs in Biomedicine, 74**:** 63-67

Krzan, M., Stenovec, M., Kreft, M., Pangrsic, T., Grilc, S., Haydon, P.G., Zorec, R., 2003. Calcium-dependent exocytosis of atrial natriuretic peptide from astrocytes. Journal of Neuroscience, 23**:** 1580-1583

Laage, R., Langosch, D., 1997. Dimerization of the synaptic vesicle protein synaptobrevin (vesicle-associated membrane protein) II depends on specific residues within the transmembrane segment. European Journal of Biochemistry, 249**:** 540-546

Lehninger, A.L., 1975. Biochemistry : the molecular basis of cell structure and function, Vol., Worth Publishers, 4th ed. New York: 167 p

Li, F., Pincet, F., Perez, E., Eng, W.S., Melia, T.J., Rothman, J.E., Tareste, D., 2007. Energetics and dynamics of SNAREpin folding across lipid bilayers. Nature Structural and Molecular Biology, 14**:** 890-896

Maienschein, V., Marxen, M., Volknandt, W., Zimmermann, H., 1999. A plethora of presynaptic proteins associated with ATP-storing organelles in cultured astrocytes. Glia, 26**:** 233-244

Malarkey, E.B., Parpura, V., 2008. Mechanisms of glutamate release from astrocytes. Neurochemistry International, 52**:** 142-154

Malarkey, E.B., Parpura, V., 2011. Temporal characteristics of vesicular fusion in astrocytes: examination of synaptobrevin 2-laden vesicles at single vesicle resolution. Journal of Physiology, 589**:** 4271-4300

Melcangi, R.C., Galbiati, M., Messi, E., Magnaghi, V., Cavarretta, I., Riva, M.A., Zanisi, M., 1997. Astrocyte-neuron interactions in vitro: role of growth factors and steroids on LHRH dynamics. Brain Research Bulletin, 44**:** 465-469

Miesenbock, G., De Angelis, D.A., Rothman, J.E., 1998. Visualizing secretion and synaptic transmission with pH-sensitive green fluorescent proteins. Nature, 394**:** 192-195

Miesenbock, G., 2012. Synapto-pHluorins: genetically encoded reporters of synaptic transmission. Cold Spring Harbor Protocols, 2012**:** 213-217

Miyawaki, A., Llopis, J., Heim, R., McCaffery, J.M., Adams, J.A., Ikura, M., Tsien, R.Y., 1997. Fluorescent indicators for Ca^{2+} based on green fluorescent proteins and calmodulin. Nature, 388**:** 882-887

Mohrmann, R., de Wit, H., Verhage, M., Neher, E., Sorensen, J.B., 2010. Fast vesicle fusion in living cells requires at least three SNARE complexes. Science, 330**:** 502-505

Molchanova, S.M., Oja, S.S., Saransaari, P., 2007. Inhibitory effect of taurine on veratridine-evoked D-[3H]aspartate release from murine corticostriatal slices: involvement of chloride channels and mitochondria. Brain Research, 1130**:** 95-102

Mothet, J.P., Pollegioni, L., Ouanounou, G., Martineau, M., Fossier, P., Baux, G., 2005. Glutamate receptor activation triggers a calcium-dependent and SNARE protein-dependent release of the gliotransmitter D-serine. Proceedings of the National Academy Sciences U S A, 102**:** 5606-5611

Nagai, T., Ibata, K., Park, E.S., Kubota, M., Mikoshiba, K., Miyawaki, A., 2002. A variant of yellow fluorescent protein with fast and efficient maturation for cell-biological applications. Nature Biotechnology, 20**:** 87-90

Nedergaard, M., Ransom, B., Goldman, S.A., 2003. New roles for astrocytes: redefining the functional architecture of the brain. Trends in Neurosciences, 26**:** 523-530

Ngatchou, A.N., Kisler, K., Fang, Q., Walter, A.M., Zhao, Y., Bruns, D., Sorensen, J.B., Lindau, M., 2010. Role of the synaptobrevin C terminus in fusion pore formation. Proceedings of the National Academy of Sciences U S A, 107**:** 18463-18468

O'Connor, V., Lee, A.G., 2002. Synaptic vesicle fusion and synaptotagmin: 2B or not 2B? Nature Neuroscience, 5**:** 823-824

Oyler, G.A., Higgins, G.A., Hart, R.A., Battenberg, E., Billingsley, M., Bloom, F.E., Wilson, M.C., 1989. The identification of a novel synaptosomal-associated protein, SNAP-25, differentially expressed by neuronal subpopulations. Journal of Cell Biology, 109**:** 3039-3052

Parpura, V., Basarsky, T.A., Liu, F., Jeftinija, K., Jeftinija, S., Haydon, P.G., 1994. Glutamate-mediated astrocyte-neuron signalling. Nature, 369**:** 744-747

Parpura, V., Baker, B.J., Jeras, M., Zorec, R., 2010. Regulated exocytosis in astrocytic signal integration. Neurochemistry International, 57**:** 451-459

Parpura, V., Zorec, R., 2010. Gliotransmission: Exocytotic release from astrocytes. Brain Research Reviews, 63**:** 83-92

Pawley, J.B., Masters, R.B.R., 1996. Handbook of Biological Confocal Microscopy, Second Edition. Optical Engineering, 35**:** 2765-2766

Pickel, V.M., Chan, J., Milner, T.A., 1989. Ultrastructural basis for interactions between central opioids and catecholamines. II. Nuclei of the solitary tracts. Journal of Neuroscience, 9**:** 2519-2535

Pickel, V.M., Chan, J., 1999. Ultrastructural localization of the serotonin transporter in limbic and motor compartments of the nucleus accumbens. Journal of Neuroscience, 19**:** 7356-7366

Potokar, M., Stenovec, M., Kreft, M., Kreft, M.E., Zorec, R., 2008. Stimulation inhibits the mobility of recycling peptidergic vesicles in astrocytes. Glia, 56**:** 135-144

Potokar, M., Stenovec, M., Gabrijel, M., Li, L., Kreft, M., Grilc, S., Pekny, M., Zorec, R., 2010. Intermediate filaments attenuate stimulation-dependent mobility of endosomes/lysosomes in astrocytes. Glia, 58**:** 1208-1219

Qu, L., Akbergenova, Y., Hu, Y., Schikorski, T., 2009. Synapse-to-synapse variation in mean synaptic vesicle size and its relationship with synaptic morphology and function. Journal of Computational Neurology, 514**:** 343-352

Rizzo, M.A., Davidson, M.W., Piston, D.W., 2009a. Fluorescent protein tracking and detection: applications using fluorescent proteins in living cells. Cold Spring Harbor Protocols, 2009**:** 1-13

Rizzo, M.A., Davidson, M.W., Piston, D.W., 2009b. Fluorescent protein tracking and detection: fluorescent protein structure and color variants. Cold Spring Harbor Protocols, 2009**:** 1-21

RodrĂ-guez, P.F., Blandin, P., Maksimovic, I., Sepulveda, E., Muro, E., Dubertret, B., Loriette, V., 2009. High-resolution fluorescence microscopy using three-

dimensional structured illumination. In: European Conference on Biomedical Optics. Optical Society of America, 7367**:** 73670X1-7

Rollenhagen, A., Satzler, K., Rodriguez, E.P., Jonas, P., Frotscher, M., Lubke, J.H., 2007. Structural determinants of transmission at large hippocampal mossy fiber synapses. Journal of Neuroscience, 27**:** 10434-10444

Roos, A., Boron, W.F., 1981. Intracellular pH. Physiological Reviews, 61**:** 296-434

Rust, M.J., Bates, M., Zhuang, X., 2006. Sub-diffraction-limit imaging by stochastic optical reconstruction microscopy (STORM). Nature Methods, 3**:** 793-795

Sankaranarayanan, S., De Angelis D Fau - Rothman, J.E., Rothman Je Fau - Ryan, T.A., Ryan, T.A., 2000. The use of pHluorins for optical measurements of presynaptic activity. Biophysical Journal, 79**:** 2199-2208

Schermelleh, L., Carlton, P.M., Haase, S., Shao, L., Winoto, L., Kner, P., Burke, B., Cardoso, M.C., Agard, D.A., Gustafsson, M.G., Leonhardt, H., Sedat, J.W., 2008. Subdiffraction multicolor imaging of the nuclear periphery with 3D structured illumination microscopy. Science, 320**:** 1332-1336

Schoch, S., Deak, F., Konigstorfer, A., Mozhayeva, M., Sara, Y., Sudhof, T.C., Kavalali, E.T., 2001. SNARE function analyzed in synaptobrevin/VAMP knockout mice. Science, 294**:** 1117-1122

Schwartz, J.P., Wilson, D.J., 1992. Preparation and characterization of type 1 astrocytes cultured from adult rat cortex, cerebellum, and striatum. Glia, 5**:** 75-80

Shroff, H., Galbraith, C.G., Galbraith, J.A., White, H., Gillette, J., Olenych, S., Davidson, M.W., Betzig, E., 2007. Dual-color superresolution imaging of genetically expressed probes within individual adhesion complexes. Proceedings of the National Academy of Sciences U S A, 104**:** 20308-20313

Sinha, R., Ahmed, S., Jahn, R., Klingauf, J., 2011. Two synaptobrevin molecules are sufficient for vesicle fusion in central nervous system synapses. Proceedings of the National Academy of Sciences U S A, 108**:** 14318-14323

Sollner, T., Bennett, M.K., Whiteheart, S.W., Scheller, R.H., Rothman, J.E., 1993. A protein assembly-disassembly pathway in vitro that may correspond to sequential steps of synaptic vesicle docking, activation, and fusion. Cell, 75**:** 409-418

Stryer, L., 1995. Biochemistry, Vol., W.H. Freeman, 5th Edition, New York: 463 p.

Sutton, R.B., Fasshauer, D., Jahn, R., Brunger, A.T., 1998. Crystal structure of a SNARE complex involved in synaptic exocytosis at 2.4 Å resolution. Nature, 395**:** 347-353

Szatkowski, M., Barbour, B., Attwell, D., 1990. Non-vesicular release of glutamate from glial cells by reversed electrogenic glutamate uptake. Nature, 348**:** 443-446

Takahashi, N.K., Haruo, 2007. Exocytic process analyzed with two-photon excitation imaging in endocrine pancreas. Endocrine Journal, 54**:** 337-346

Takamori, S., Holt, M., Stenius, K., Lemke, E.A., Gronborg, M., Riedel, D., Urlaub, H., Schenck, S., Brugger, B., Ringler, P., Muller, S.A., Rammner, B., Grater, F., Hub, J.S., De Groot, B.L., Mieskes, G., Moriyama, Y., Klingauf, J., Grubmuller, H., Heuser, J., Wieland, F., Jahn, R., 2006. Molecular anatomy of a trafficking organelle. Cell, 127**:** 831-846

Trimble, W.S., Scheller, R.H., 1988. Molecular biology of synaptic vesicle-associated proteins. Trends in Neurosciences, 11**:** 241-242

van den Bogaart, G., Holt, M.G., Bunt, G., Riedel, D., Wouters, F.S., Jahn, R., 2010. One SNARE complex is sufficient for membrane fusion. Nature Structural and Molecular Biology, 17**:** 358-364

Vardjan, N., Stenovec, M., Jorgacevski, J., Kreft, M., Zorec, R., 2007. Elementary properties of spontaneous fusion of peptidergic vesicles: fusion pore gating. Journal of Physiology, 585**:** 655-661

Warr, O., Takahashi, M., Attwell, D., 1999. Modulation of extracellular glutamate concentration in rat brain slices by cystine-glutamate exchange. Journal of Physiology, 514**:** 783-793

Westergaard, N., Drejer, J., Schousboe, A., Sonnewald, U., 1996. Evaluation of the importance of transamination versus deamination in astrocytic metabolism of [U-13C]glutamate. Glia, 17**:** 160-168

Wienisch, M., Klingauf, J., 2006. Vesicular proteins exocytosed and subsequently retrieved by compensatory endocytosis are nonidentical. Nature Neuroscience, 9**:** 1019-1027

Wildanger, D., Medda, R., Kastrup, L., Hell, S.W., 2009. A compact STED microscope providing 3D nanoscale resolution. Journal of Microscoscopy, 236**:** 35-43

Willig, K.I., Rizzoli, S.O., Westphal, V., Jahn, R., Hell, S.W., 2006. STED microscopy reveals that synaptotagmin remains clustered after synaptic vesicle exocytosis. Nature, 440**:** 935-939

Wilson, T., 2011a. Resolution and optical sectioning in the confocal microscope. Journal of Microscopy, 244**:** 113-121

Wilson, T., 2011b. Optical sectioning in fluorescence microscopy. Journal of Microscopy, 242**:** 111-116

Wolosker, H., Sheth, K.N., Takahashi, M., Mothet, J.P., Brady, R.O., Jr., Ferris, C.D., Snyder, S.H., 1999. Purification of serine racemase: biosynthesis of the neuromodulator D-serine. Proceedings of the National Academy Sciences U S A, 96**:** 721-725

Woo, D.H., Han, K.S., Shim, J.W., Yoon, B.E., Kim, E., Bae, J.Y., Oh, S.J., Hwang, E.M., Marmorstein, A.D., Bae, Y.C., Park, J.Y., Lee, C.J., 2012. TREK-1 and Best1 channels mediate fast and slow glutamate release in astrocytes upon GPCR activation. Cell, 151**:** 25-40

Xu, J., Peng, H., Kang, N., Zhao, Z., Lin, J.H., Stanton, P.K., Kang, J., 2007. Glutamate-induced exocytosis of glutamate from astrocytes. Journal of Biological Chemistry, 282**:** 24185-24197

Ye, Z.C., Wyeth, M.S., Baltan-Tekkok, S., Ransom, B.R., 2003. Functional hemichannels in astrocytes: a novel mechanism of glutamate release. Journal of Neuroscience, 23**:** 3588-3596

Zhang, B., Koh, Y.H., Beckstead, R.B., Budnik, V., Ganetzky, B., Bellen, H.J., 1998. Synaptic vesicle size and number are regulated by a clathrin adaptor protein required for endocytosis. Neuron, 21**:** 1465-1475

Zinchuk, V., Grossenbacher-Zinchuk, O., 2009. Recent advances in quantitative colocalization analysis: focus on neuroscience. Progress in Histochemistry and Cytochemistry, 44**:** 125-172

ACKNOWLEDGMENTS

First of all I would like to thank my PhD supervisor Prof. Robert Zorec for giving me the opportunity to work in his group, for exposing me to the exciting field of glia, for the motivation to undertake challenging project and at the same time for being a very patient mentor. His incredible urge to know the outcome of experiments, his openness to new ideas, the liberty to try unconventional experiments and the high level of enthusiasm about the results has made my PhD research a great learning experience.

I am grateful to the members of my thesis committee, Prof. Marko Kreft for his continuous support and valuable advice on my project and Prof. Aleš Iglič for his suggestions during the thesis meetings. I also thank Dr. Maja Potokar for her fruitful comments editing my thesis.

I would like to thank the members of our research group LN-MCP (Laboratory of Endocrinology – Molecular Cell Physiology) for creating a lively working environment both intellectually and friendly. I thank Dr. Maja Potokar and Dr. Jernej Jorgačevski for their help and advice. I thank Dr. Boštjan Rituper for his kind help with Endnote software. I thank Dr. Saša Trkov for the isolation and the routine up-keeping of the astrocytes cultures. I am also thankful to Dr. Helena Chowdhury Haque, Dr. Nina Vardjan and Dr. Matjaž Stenovec for extending all possible help and making my work easier while working in the laboratory. I would like to acknowledge members of the Institute of Pathophysiology for a fruitful support.

I would like to express my gratitude to all my friends for their moral support over the years. Last but not the least I would like to thank my parents and my brother for their love and support all along.

INDEX OF ANNEXES

Fig. I: Sb2 with enhanced yellow fluorescent protein (EYFP) based pH sensor.

Fig. II: Plasmid maps of Sb2 fusion proteins with two fluorescent proteins and their orientation in a secretory vesicle.

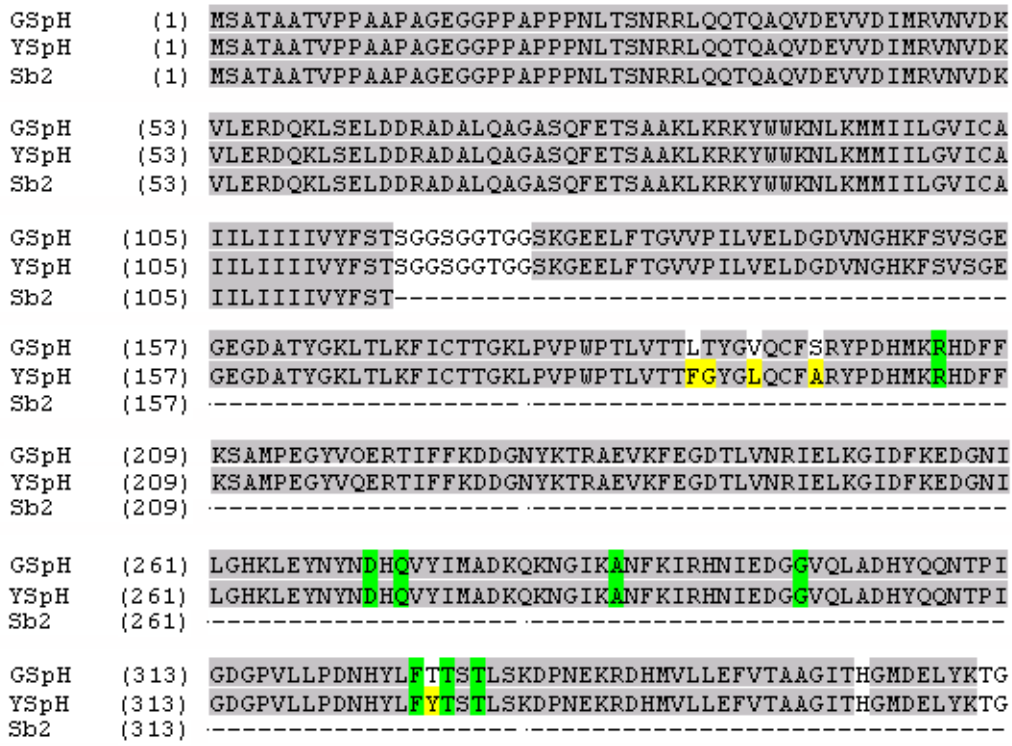

Figure I: Sb2 with enhanced yellow fluorescent protein (EYFP) based pH sensor. Alignment of yellow supercliptic synaptopHluorin (YSpH) and relevant sequences: GSpH, green supercliptic synaptopHluorin and Sb2. Amino Acids highlighted in green are those important for supercliptic pHluorin activity and those in yellow produce the yellow shifted emission. Grey shaded amino acids indicate residues for which the sequences shown are the same as in YSpH. Please note that the M in the beginning of pHluorin is changed to G and that there is the 8 aa linker (SGGSGGTG) between Sb2 and pHluorin (aa 117-124 of GSpH and YSpH) (Prof. Parpura, University of Alabama, Alabama).

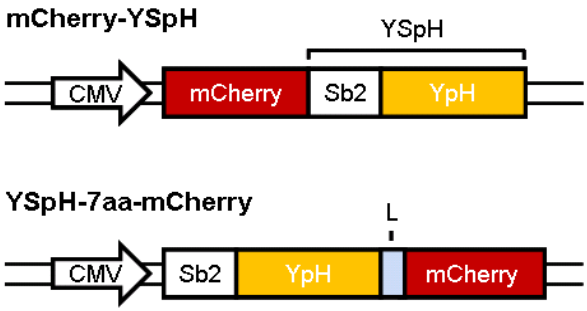

Figure II: Plasmid maps of Sb2 fusion proteins with two fluorescent proteins and their orientation in a secretory vesicle. Plasmid maps: Top) mCherry-YSpH construct has mCherry on the N-terminus of Sb2 and yellow shifted pHluorin (YpH) on its C-terminus. Bottom) YSpH-7aa-mCherry plasmid has both fluorescent proteins at the C-terminus of Sb2. mCherry is appended to the C-terminus of YSpH by the polypeptide linker (L) containing 7 amino acids (SGLRSRA). Both constructs are expressed under the control of the cytomegalovirus (CMV) promoter.